Determining the COB Location along the Iberian Margin and Galicia Bank from Gravity Anomaly Inversion, Residual Depth Anomaly and Subsidence Analysis

Leanne Cowie[1], Nick Kusznir[1] and Gianreto Manatschal[2]

[1] Earth, Ocean and Ecological Sciences, University of Liverpool, Liverpool, L69 3BX, UK

[2] *EOST-CGS (UMR 7517) CNRS, Université Louis Pasteur, 1 rue Blessig, F-67064 Strasbourg Cedex, France*

Abbreviated Title: Determining the COB Location along the Iberian Margin

Corresponding Author: Leanne Cowie

Address: Earth, Ocean and Ecological Sciences, University of Liverpool, Liverpool, L69 3BX, UK

Email: leanne.cowie.87@gmail.com

Phone: 07765673285

Summary

Knowledge and understanding of the ocean continent transition (OCT) structure, continent-ocean boundary (COB) location and crustal type are of critical importance in evaluating rifted continental margin formation and evolution. OCT structure, COB location and magmatic type also have important implications for the understanding of the geodynamics of continental breakup and in the evaluation of petroleum systems in deep-water frontier oil and gas exploration at rifted continental margins. Mapping the distribution of thinned continental crust and lithosphere, its distal extent and the start of unequivocal oceanic crust and hence determining the OCT structure and COB location at rifted continental margins is therefore a generic global problem. In order to assist in the determination of the OCT structure and COB location, we present methodologies using gravity anomaly inversion, residual depth anomaly (RDA) analysis and subsidence analysis, which we apply to the west Iberian rifted continental margin. The west Iberian margin has one of the most complete data sets available for deep magma-poor rifted margins, so there is abundant data to which the results can be calibrated. Gravity anomaly inversion has been used to determine Moho depth, crustal basement thickness and continental lithosphere thinning; subsidence analysis has been used to determine the distribution of continental lithosphere thinning; and RDAs have been used to investigate the OCT bathymetric anomalies with respect to expected oceanic bathymetries at rifted continental margins. These quantitative analytical techniques have been applied to the west Iberian rifted continental margin along profiles IAM9, Lusigal 12 (with the TGS-extension) and ISE-01. Our predictions of OCT structure, COB location and magmatic type (i.e. the volume of magmatic addition, whether the margin is 'normal' magmatic, magma-starved or magma-rich) have been tested and validated using ODP wells (Legs 103, 149 and 173), which provide observational constraints on the west Iberian margin.

Key Words:

1. Continental margins: divergent
2. Gravity anomalies and earth structure
3. Dynamics: gravity and tectonics

1. Introduction

Knowledge of the structure of the ocean continent transition (OCT), the location of the continent ocean boundary (COB), magmatic type (i.e. the volume of magmatic addition, whether the margin is 'normal' magmatic, magma-poor or magma-rich) and the distribution of oceanic and continental lithosphere are key to understanding present day rifted continental margin architecture and evolution. Rifted continental margins can be categorized into three primary magmatic types: 'normal' magmatic and two end members: magma-poor and magma-rich. A 'normal' magmatic rifted continental margin has magmatic addition, which results in oceanic crust of approximately 7km in thickness (White et al., 1992). Magma-poor rifted continental margins are often characterized by a wide OCT, extreme crustal thinning accompanied by normal faulting (Boillot et al., 1980; Manatschal, 2004; Reston, 2009) and anomalously small fractions of magmatism leading to mantle exhumation prior to oceanic spreading (Pérez-Gussinyé, 2012). Magma-rich margins are characterized by thick wedges of volcanic flows (Hinz, 1981), shown on seismic data as seaward dipping reflectors (SDRs), large amounts of syn-rift magmatic extrusives and intrusives (Coffin and Eldholm, 1994), high velocity lower crust seaboard of the continental rifted margin (Franke, 2013), and the crustal thinning may occur over a short distance. The determination of rifted continental margin magmatic type and OCT structure, which show great diversity globally, are important for understanding the geodynamic, tectonic and magmatic processes involved in rifted continental margin formation and their evolution to the present day. Understanding structure and formation processes of rifted continental margins is important, not only because they are a key component of the plate tectonic Wilson cycle (Wilson, 1966) but also for deep-water hydrocarbon exploration. In this paper, we present a set of integrated quantitative analysis techniques for assisting in the determination of OCT structure, COB location and crustal type at rifted continental margins, which have been applied and tested on the west Iberian rifted continental margin, where independent observations from ODP wells are available for ground-truthing.

Numerous studies (e.g. Zalán et al. (2011); Autin et al. (2010); Unternehr et al. (2010); Reston (2009); White et al. (2008); D'Acremont et al. (2005); Contrucci et al. (2004); Hopper et al. (2004); Chian et al. (1999); Pickup et al. (1996); Whitmarsh and Miles (1995)) have used various approaches to determine OCT structure and COB location of rifted continental margins. Techniques that have been used include the analysis of seismic reflection and refraction data, gravity and magnetic anomalies, bathymetric breaks and well data. The aims of these studies have focussed on: (i) distinguishing whether the OCT at a rifted continental margin is narrow or wide; (ii) determining the location of the distal extent of continental crust and the presence of any isolated ribbons of thinned continental crust and (iii) determining the magmatic type of a rifted continental margin.

The west Iberian rifted continental margin has abundant observational data; including seismic reflection and refraction surveys, magnetic anomalies and ODP well data. As a consequence it is a good natural laboratory for studying rifted continental margin evolution and has been used to demonstrate and test the methodologies and techniques used in this paper to determine OCT structure, COB location and magmatic type. On the west Iberian rifted continental margin, there have been many studies, which have addressed these and other questions. The application of seismic reflection and refraction data (e.g. Dean et al. (2000); Pickup et al. (1996); Whitmarsh et al. (1996)) and also seismic tomography (e.g. Zelt et al. (2003)) has focussed on the determination of the OCT structure and the identification of the inner and outer bounds of the OCT. Detailed seismic mapping and borehole data has also been applied in order to further constrain the crustal type (e.g. Péron-Pinvidic et al. (2007)), whilst magnetic anomalies have been used to tentatively locate the COB (e.g. Bronner et al. (2011)). The determination of the magmatic type of a margin has been further constrained using seismic reflection data, magnetic anomalies and ODP well data as discussed in Pickup et al. (1996).

In this study, we have applied an integrated quantitative analysis of gravity anomaly inversion, residual depth anomaly (RDA) and subsidence analysis to the west Iberian rifted continental margin.

98 Gravity anomaly inversion, incorporating a lithosphere thermal gravity anomaly correction, has been
99 used to determine crustal basement thickness, Moho depth and continental lithosphere thinning
100 across the west Iberian rifted continental margin. Sediment corrected RDAs have been used to
101 calculate departures from standard oceanic water depths, as predicted by Crosby et al. (2006) and
102 Stein and Stein (1992), whilst subsidence analysis has been used to give the distribution of
103 continental lithosphere thinning. These techniques have been interpreted individually and together
104 to identify the distribution of oceanic and thinned continental crust in order to determine the
105 structure of the OCT and locate the COB.

106 The west Iberian margin is the result of rifting and continental breakup between the North American
107 and Iberian plates during the Late Triassic to Early Cretaceous (Manatschal, 2004; Manatschal et al.,
108 2001; Péron-Pinvidic et al., 2007; Russell and Whitmarsh, 2003). The Iberian Abyssal Plain is part of
109 the magma-poor west Iberian margin (Chian et al., 1999) and is considered to be a type example of a
110 sediment-starved magma-poor rifted continental margin (Sutra and Manatschal, 2012). The west
111 Iberian margin is subdivided into three main sections: Galicia margin to the north, the Iberian
112 Abyssal Plain in the middle and the Tagus Abyssal Plain to the south (Manatschal et al., 2001). This
113 paper focuses on three key profiles (IAM9, Lusigal 12 and ISE-01) along the Iberian Abyssal Plain and
114 the Galicia margin highlighted in Figure 1(a). The west Iberian rifted continental margin is, at
115 present, considered to be one of the best studied rifted continental margins world-wide due to the
116 abundant observational data available in the form of deep sea drilling (ODP Legs 103, 149 and 173)
117 (Boillot et al., 1987; Sawyer et al., 1994; Tucholke et al., 2007; Whitmarsh et al., 1998; Whitmarsh
118 and Sawyer, 1996) combined with seismic reflection and refraction surveys (Manatschal et al., 2010).

119 Within the literature there are a range of different definitions of the OCT and COB (e.g. Péron-
120 Pinvidic et al. (2007), Whitmarsh and Miles (1995), Manatschal et al. (2001), Dean et al. (2000)
121 Manatschal et al. (2010) and Discovery 215 Working Group (1998). Within this paper, however, we
122 define the OCT as the region between unequivocal continental crust of 'normal' thickness and

unequivocal oceanic crust; the lithosphere in this region is highly thinned, with complex tectonics, variable magmatism and possible mantle exhumation. We define the COB as the distal limit of unequivocal continental crust; however, determining the location of the COB is made difficult by the presence of exhumed mantle and complex tectonics. Another important term used is continental breakup age. Conceptually the term continental breakup may be used to either describe the point at which the continental crust ruptures and starts to separate, or when plate boundaries are localised by the onset of decompression melting and magmatic seafloor spreading. Within this paper, we use the latter definition (i.e. when plate boundaries are localised by the onset of decompression melting and magmatic seafloor spreading).

2. OCT Structure: Profile IAM9

Integrated quantitative analysis has been used to determine OCT structure, COB location and magmatic type along profile IAM9 (A-A'). Profile IAM9 has been used to describe the gravity anomaly inversion, RDA and subsidence analysis techniques in detail due to the availability of reliable seismic Moho depths (Dean et al., 2000), which are required for calibration of the reference Moho depth.

2.1. Crustal Basement Thickness and Continental Lithosphere Thinning along IAM9 from Gravity Anomaly Inversion

Gravity anomaly inversion has been used to determine crustal basement thickness, Moho depth and continental lithosphere thinning, which in turn give the distribution of oceanic and continental lithosphere. The data used within the gravity anomaly inversion are bathymetry (Amante and Eakins, 2009) (Figure 1(a)), satellite derived free air gravity (Sandwell and Smith, 2009) (Figure 1(b)), 2D sediment thickness from wide angle seismic data (Dean et al., 2000) (Figure 2(a)) and ocean age isochrons from Müller et al. (1997).

146 The gravity anomaly inversion method is carried out in the 3D spectral domain, using the scheme of
147 Parker (1972) to predict Moho depth and hence determine crustal basement thickness. As the
148 gravity anomaly inversion has been applied to rifted continental margin lithosphere, a lithosphere
149 thermal gravity anomaly correction is incorporated to account for the elevated geothermal gradient
150 within oceanic and rifted continental margin lithosphere. Failure to include the correction for the
151 lithosphere thermal gravity anomaly can lead to predictions of Moho depth and crustal basement
152 thickness at rifted continental margins, which are substantially too great. The results from gravity
153 anomaly inversion are dependent on the age of continental breakup due to the lithosphere thermal
154 gravity anomaly correction being dependent on the lithosphere thermal re-equilibration time. Some
155 papers consider the age of breakup for the west Iberian margin to be at the Aptian-Albian boundary,
156 112Ma (Péron-Pinvidic et al., 2007); whereas others consider an older breakup age of 126Ma,
157 (Manatschal, 2004; Russell and Whitmarsh, 2003). As the gravity anomaly inversion requires a
158 definitive breakup age, a Cretaceous breakup age of 120Ma, which is within this proposed range, has
159 been used. Changing the breakup age used within the gravity anomaly inversion to the maximum
160 breakup age proposed, 126Ma, or to the minimum breakup age proposed, 112Ma, has a small effect
161 on the results, but does not substantially change the overall conclusions. A more detailed
162 description of the gravity anomaly inversion technique methodology is given in Cowie and Kusznir
163 (2012), Alvey et al. (2008), Chappell and Kusznir (2008) and Greenhalgh and Kusznir (2007).

164 Within the gravity anomaly inversion the reference Moho depth is an important parameter that
165 requires careful consideration and calibration. The 3D gravity anomaly inversion technique
166 determines 3D Moho relief; the absolute Moho depth requires, in addition, a reference datum which
167 is the reference Moho depth. The long wavelength components of the Earth's gravity anomaly field
168 are controlled by deep mantle dynamic processes and are not related to lithosphere and crustal
169 structure, and as a consequence the reference Moho depth varies globally. It is therefore necessary
170 for the reference Moho depth to be determined by calibration against seismic refraction Moho

depths to ensure the correct reference Moho depth is used within the gravity anomaly inversion (Cowie and Kusznir, 2012); within this paper calibration has only been done using seismic refraction Moho depths for unequivocal oceanic crust. A crustal basement density of 2850kgm^{-3} (Carlson and Herrick, 1990; Christensen and Mooney, 1995) and a mantle density of 3300kgm^{-3} (Jordan and Anderson, 1974) are used in the gravity anomaly inversion; sensitivity tests to these values have been made and do not significantly change the conclusions.

Reference Moho depths have been calibrated, for the oceanic domain, using profile IAM9, which has reliable seismic oceanic Moho depth estimates from the wide angle seismic data of Dean et al. (2000). Sensitivities to reference Moho depths of 37.5km, 40km and 42.5km have been examined for the IAM9 profile. Moho depths predicted from gravity anomaly inversion produced for these sensitivities to reference Moho depth are shown in Figure 2(b). A reference Moho depth of 37.5km is too small as it predicts Moho depths which are too shallow and in places plot above the top basement within the sedimentary layer. A larger reference Moho depth is required; both reference Moho depths of 40km and 42.5km predict a deeper Moho. Calibration gives a reference Moho depth of 41km (inset of Figure 2(b)) in order to predict crustal basement thicknesses consistent with those seen in the wide-angle seismic data.

The gravity anomaly inversion, which is carried out in the 3D spectral domain, uses 3D bathymetry and free air gravity anomaly data, while the sediment thicknesses are derived from the 2D seismic

profiles and are interpolated between profiles in order to construct a pseudo 3D sediment volume. The results from the 3D gravity anomaly inversion are then extracted along the 2D profiles.

A crustal cross section (A-A') along profile IAM9 (Figure 2(c)), has been constructed using the bathymetry and 2D sediment thickness data (Dean et al., 2000) with the crustal basement thicknesses and Moho depths predicted from gravity anomaly inversion assuming the calibrated reference Moho depth of 41km. The crustal cross section along profile IAM9 (A-A') shows the distribution of oceanic and continental crust and hence the structure of the OCT. The red dashed line shows the 7.9kms^{-1} iso-velocity contour (Dean et al., 2000) representing the seismic Moho depth. There is a good correlation between the Moho depths predicted from gravity anomaly inversion, using the calibrated reference Moho depth of 41km, and the seismic Moho depths; crustal basement thicknesses between 5km and 7km are predicted at the western end of the profile. In the centre of the profile (between 100km and 200km) the crustal basement thicknesses predicted from gravity anomaly inversion thin considerably, to between approximately 1.5km and 2km, and the gravity anomaly inversion predicts a shallower Moho depth than predicted by the 7.9kms^{-1} iso-velocity contour. The start of the necking zone again shows a good correlation between the Moho depths predicted from gravity anomaly inversion and the seismic Moho depths. Under the continental crust inboard of the necking zone there is a significant difference between the gravity anomaly inversion predicted Moho depths and the Moho depths predicted by Dean et al. (2000). The difference, in part, can be attributed to a too thin estimate of sediment thickness in this region used within our gravity anomaly inversion, which results in the gravity anomaly inversion predicted Moho being too deep. (Dean et al., 2000) states that the crustal thicknesses at the continental end of the profile are from 2D modelling of shipboard gravity data and their shallower Moho could also be the result of using lower crustal basement densities than those used within our gravity anomaly inversion.

The distribution of continental lithosphere thinning predicted from gravity anomaly inversion has also been used along the west Iberian rifted continental margin. During continental rifting and breakup there can be a significant addition of magmatic material to the crust. The thickness of the crustal magmatic addition is estimated using the parameterization of decompression melting model of White & McKenzie (1989), from the continental lithosphere thinning factor (γ) determined from gravity anomaly inversion, where

$$\gamma = 1 - \frac{1}{\beta} \quad (1)$$

This parameterisation of decompression melting is described in detail in Chappell & Kusznir (2008). Decompression melting results in magmatic addition, which leads to the generation of oceanic crust and also magmatic under-plating and extrusives, e.g. seaward dipping reflectors (SDRs) at many rifted continental margins (at the west Iberian margin SDRs are not observed). 'Normal' decompression melting produces a 7km thick oceanic crust with the initiation of decompression melting occurring at γ=0.7 and a maximum magmatic addition of 7km at a thinning factor of 1.0 (for $\beta=\infty$). We also consider the case of a magma-starved margin where no magmatic addition to the crust is generated. In the case of magma-starved margins, serpentinization of exhumed mantle occurs. Therefore, we also consider a solution for mantle serpentinization, applicable to magma-starved margins, in which serpentinization begins at approximately γ=0.7 (corresponding to approximately 10km thick crust) and at γ=1.0 generates a serpentinized mantle with a mass deficiency with respect to mantle equivalent to crustal basement of thickness 3km. This estimate of the equivalent mass deficiency of serpentinized mantle is described in Appendix A.

Continental lithosphere thinning factor (γ) estimates for profile IAM9, derived from gravity anomaly inversion assuming three different solutions, are shown in Figure 2(d). A magma-starved solution; a 'normal' magmatic solution and a solution for serpentinized mantle have been examined. Continental lithosphere thinning factors of zero indicate that there has been no stretching or

thinning of the continental lithosphere, whereas a continental lithosphere thinning factor of one indicates that there has been infinite stretching and thinning of the original continental lithosphere and there is no continental lithosphere (or crust) remaining. Changes in the continental lithosphere thinning factors, determined from gravity anomaly inversion, specifically changes from high thinning factors (between 0.9 and 1.0) to lower thinning factors, may be used to constrain the COB and necking zone location along the profile lines. Along profile IAM9 (Figure 2(d)), the continental lithosphere thinning factors from gravity anomaly inversion for 'normal' magmatic addition are 1.0 along most of the profile (they begin to decrease at approximately 260km distance along profile); this solution probably places the COB too far inboard and is inappropriate for a magma-starved margin. The magma-starved solution, with no serpentinization, fails to reach 1.0 anywhere. The serpentinized mantle solution predicts high continental lithosphere thinning factors in the central region, which is where Dean et al. (2000) indicate that there are peridotite mantle ridges. The interpretation of these continental lithosphere thinning factor curves to constrain COB location and the presence of exhumed mantle or 'normal' oceanic crust is discussed in detail in Section 5.

2.2. Residual Depth Anomaly Analysis: Profile IAM9

2.2.1. Sediment Corrected RDA

Residual depth anomaly (RDA) analysis has been applied to the west Iberian rifted continental margin in order to examine OCT bathymetric anomalies with respect to expected oceanic bathymetries at the rifted continental margin. A RDA for oceanic crust is the difference between observed (b_{obs}) and ocean age predicted bathymetry ($b_{predicted}$). Age predicted bathymetries have been calculated using the thermal plate model predictions from Crosby and McKenzie (2009). Sensitivities to the thermal plate model predictions from Parsons and Sclater (1977) and Stein and Stein (1992) have also been examined (Figure 3(b)); RDA results computed using these different thermal plate model predictions do not vary significantly.

$$\mathrm{RDA} = \mathrm{b_{obs}} - \mathrm{b_{predicted}} \quad (2)$$

Changes in RDA signature are used to estimate the distal extent of continental crust and where unequivocal oceanic crust begins.

Sediment corrected bathymetry, used to calculate RDAs corrected for sediment loading, has been determined using flexural backstripping and decompaction. Figure 3(c) shows a comparison of the uncorrected RDA and the sediment corrected RDA along profile IAM9. Correcting for the effect of sediment loading has a considerable effect on the RDA results; the difference between the uncorrected RDA and the sediment corrected RDA is approximately 1500m at the western end of the profile. Sediment corrected bathymetry has been calculated using flexural backstripping (Kusznir et al., 1995) and comprises the removal of the sedimentary load, allowing for the flexural isostatic response and decompaction of the remaining sediments. Flexural backstripping and decompaction assumes shaly-sand compaction parameters (Sclater and Christie, 1980) during the removal of the sedimentary layer. Removal of the sedimentary layer along profile IAM9, results in a sediment corrected bathymetry that is approximately 1500m deeper than observations of present day bathymetry. The sediment corrected RDA along profile IAM9 (Figure 3(c)), is negative with a magnitude between -1000m and -1500m at the western end of the profile.

Age predicted oceanic bathymetries, used to calculate the sediment corrected RDA, are dependent on the oceanic lithospheric age. The Müller et al. (2008) global ocean age isochrons do not extend

291 the entire length of profile IAM9; it is therefore necessary to consider sensitivities to oceanic
292 lithospheric age. Two approaches have been examined: the first uses a constant value of 120Ma for
293 the profile, whilst the second uses Müller et al. (2008) age isochrons with their age gradient
294 extrapolated inboard. A comparison and sensitivity of the sediment corrected RDA results to ocean
295 age isochrons is shown in Figure 3(d), both approaches produce similar results.

296 The flexural backstripping process calculates the flexural isostatic response of the removed layer of
297 sediments. Within this calculation the effective elastic thickness (Te) controlling the flexural
298 strength of the lithosphere is considered. Te depends on the bending stresses applied to the plate,
299 the rate of stress application, the lithosphere composition and the geothermal gradient (Kusznir and
300 Karner, 1985). Te's between 1.5km and 5km have been determined for syn-rift extensional settings
301 (Roberts et al., 1998). For post-rift flexural isostatic response, Roberts et al. (1998) show that this is
302 relatively insensitive to the magnitude of Te because of the longer wavelength of post-rift sediment
303 loading compared to syn-rift. The sensitivity to Te is shown for the Iberian Abyssal Plain sediment
304 corrected RDA results in Figure 3(e); sensitivities to Te's of 1.5km, 5km and 10km have been
305 examined. Te's of 1.5km, 5km and 10km produce sediment corrected RDAs of similar magnitude; a
306 Te of 1.5km has been used due to the negligible difference in the magnitude of the sediment
307 corrected RDAs.

308 ### 2.2.2. RDA Component from Crustal Basement Thickness Variations (RDA_{CT})

309 In addition to the RDA corrected for sediment loading, the RDA component from variations in crustal
310 basement thickness (RDA_{CT}) has also been computed, which is the result of the presence of
311 anomalously thick or thin crust. Crustal basement thicknesses from gravity anomaly inversion (using
312 reference Moho depth calibrated against seismic Moho depths) are used to predict departures from
313 the average global oceanic crustal thickness of 7km (White et al., 1992). RDA_{CT} has been computed
314 using the difference between the gravity anomaly inversion predicted crustal basement thickness

(tc_{grav}) and the average global oceanic crustal basement thickness (tc_{ref}) together with Airy isostasy. The local isostatic response to variation in gravity inverted non-continental crustal thickness, from the 7km global average oceanic crustal thickness (*tcref*) is given by:

$$\mathrm{RDA_{CT}} = \frac{(\mathrm{tc_{ref}} - \mathrm{tc_{grav}})(\rho_m - \rho_c)}{(\rho_m - \rho_{infil})} \quad (3)$$

where ρ_m is the density of the mantle (3300kgm^{-3}), ρ_c is the density of the crust (2850kgm^{-3}) and ρ_{infill} is the density of the water infill (1000kgm^{-3}). Crust, which is approximately 7km thick, will have a corresponding RDA_{CT} of zero. A positive RDA_{CT} reflects crust that is thicker than 7km, whereas if the RDA_{CT} is negative, this corresponds to crust that is thinner than 7km or the presence of exhumed mantle.

The RDA_{CT} along profile IAM9 (Figure 3(f)) ranges between zero and approximately -800m at the western end and central region of the profile, and becomes more negative before increasing and becoming positive over the continental crust.

2.2.3. Comparison of Sediment Corrected RDA with RDA Component from Crustal Basement Thickness Variations

Figure 3(f) shows the sediment corrected RDA and the RDA_{CT} along profile IAM9. In oceanic regions it is expected that the RDA signal, from both the sediment corrected RDA and the RDA_{CT}, will be constant and near zero, whereas for regions of thicker continental crust inboard of the COB, it is expected that the RDA signals will become more positive. Changes in the RDA signal may be used to identify the change in crustal mass deficiency and thickness with respect to the mantle; these changes in RDA signal may also be interpreted as a change in crustal type enabling the determination of the COB location.

Both the sediment corrected RDA and the RDA_{CT} along profile IAM9 are negative in the western and central region and show the same general trend along the profile although they have different magnitudes. The difference (ΔRDA) between the sediment corrected RDA and the RDA_{CT} corresponds to the RDA corrected for both sediment loading and variations in crustal thickness away from the oceanic average.

$$\Delta\mathrm{RDA} = \text{sediment corrected RDA} - \mathrm{RDA_{CT}} \quad (4)$$

A ΔRDA of zero implies that there is no anomalous uplift or subsidence at the margin, whereas a positive ΔRDA implies anomalous uplift and a negative ΔRDA implies anomalous subsidence along a margin. The ΔRDA (Figure 3(g)) along IAM9 is between -300m and -1000m at the western end of the profile, which is equated to mantle dynamic subsidence.

2.3. Continental Lithosphere Thinning from Subsidence Analysis

Subsidence analysis has been used to determine the distribution of continental lithosphere thinning and the distal extent of continental crust in order to locate the inner and outer bounds of the OCT. Subsidence analysis involves the conversion of water loaded subsidence into continental lithosphere thinning factors, assuming McKenzie (1978). Flexural backstripping is used to give the sediment corrected bathymetry to top pre-rift and top oceanic crust (Figure 4 (b)). It is assumed that the initial datum of original continental pre-rift surface was at or near to sea level; therefore the sediment corrected bathymetry can be equated to water loaded subsidence (see comparable estimate of tectonic subsidence from Henning et al. (2004)). Water loaded subsidence is interpreted as the sum of initial (Si) and thermal (St) subsidence in the context of the McKenzie (1978) intra-continental rift model. A correction for magmatic addition due to adiabatic decompression (White and McKenzie, 1989) during continental rifting and seafloor spreading has been included (see Roberts et al. (2013)) and uses the same scheme as described earlier in the gravity anomaly

359 inversion section. Magmatic addition from decompression melting results in thicker crust due to
360 volcanic intrusion and extrusion, which isostatically reduces the initial subsidence as predicted by
361 McKenzie (1978) and corresponds to the formation of oceanic crust. Magmatic addition also
362 increases the thickness of the crust thinned by lithosphere stretching.

363 Initial subsidence corresponds to the isostatic response of the crustal thinning and thermal loads at
364 the time of rifting, which is assumed to be instantaneous; whilst total subsidence corresponds to the
365 isostatic response of the crustal thinning and thermal loads after a defined time in the post-rift.
366 Sensitivity tests using upper and lower bounds of the time of breakup (126 and 112 Ma) have been
367 examined and the results are not significantly different. The crustal thinning load is assumed to be
368 constant after rifting, while the thermal subsidence varies with time due to the dissipation of the
369 syn-rift lithosphere thermal anomaly. Instantaneous rifting is assumed, which allows the
370 comparison of the numerically calculated total subsidence from flexural backstripping with that
371 analytically calculated using McKenzie (1978) modified for magmatic additions. Magmatic additions
372 due to decompression melting modify the predicted relationship between continental lithosphere
373 thinning factor (γ) and water loaded subsidence. Water loaded subsidence is inverted using the
374 'normal' magmatic curve (Figure 4(c)) magma poor and serpentinized mantle curves (Figure 4(d)) to
375 give continental lithosphere thinning factors. The subsidence analysis methodology assumes depth
376 uniform stretching and thinning, as a consequence thinning factors for continental lithosphere and
377 crust are identical. The isostatic response of mantle serpentinization is described in Appendix A, and
378 is estimated to be equivalent to crustal basement of approximately 3km thickness.

379 Continental lithosphere thinning factors from subsidence analysis along profile IAM9 are shown in
380 Figure 4(e). For the west Iberian margin, a 'normal' magmatic solution, a magma-starved solution
381 and a solution for serpentinized mantle are examined. A 'normal' magmatic solution predicts
382 continental lithosphere thinning factors of 1.0 everywhere outboard of the necking zone, while the
383 magma-starved solution, with no serpentinization, predicts continental lithosphere thinning factors

between 0.8 and 1. The solution for serpentinized mantle lies between these two and is more appropriate to a magma poor margin. Continental lithosphere thinning factors derived from subsidence analysis can be used to determine COB location and crustal type which is discussed in Section 5.

Continental lithosphere thinning factors predicted from gravity anomaly inversion are generally less than those predicted from subsidence analysis. This difference can be attributed to dynamic topography, as the gravity anomaly inversion results have been calibrated and include a correction for dynamic topography, whereas the subsidence analysis results do not.

The subsidence analysis for IAM9 by Henning et al. (2004) uses a different approach, predicting crustal thickness variation; as a consequence our results are not easily compared.

3. OCT Structure along the Lusigal 12 Profile

3.1. Crustal Basement Thickness and Continental Lithosphere Thinning along Lusigal 12 from Gravity Anomaly Inversion

Gravity anomaly inversion has been applied to the Lusigal 12 profile (with the TGS extension; see Sutra et al. (2013)(2013)(2013)(2013)(2013)(2013)(2013)(2013)(2013)(2013) in order to determine the crustal basement thickness, Moho depth and continental lithosphere thinning along profile. Within the gravity anomaly inversion the calibrated reference Moho depth of 41km, from IAM9, has been assumed to be applicable due to the proximity of Lusigal 12 to IAM9. Crustal cross section (B-B') along profile Lusigal 12 (Figure 5(b)) is constructed using bathymetry, sediment thickness (Sutra and Manatschal, 2012) (Figure 5(a)) and predicted Moho depths from gravity anomaly inversion. Using the calibrated reference Moho depth of 41km, the gravity anomaly inversion predicts thin crust of between 2km and 4km thickness at the western end of the profile.

Continental lithosphere thinning factors (γ) predicted from gravity anomaly inversion are shown in Figure 5(c). Sensitivities to a magma-starved solution, a 'normal' magmatic solution and a solution for serpentinized mantle have been examined. Continental lithosphere thinning factors from gravity anomaly inversion show high thinning factors for all three solutions at the western end of the profile. Continental lithosphere thinning factors for a 'normal' magmatic solution saturate at 1.0 in the central and western section of the profile. If a 'normal' magmatic solution is applicable to this profile, it suggests that this region is all oceanic. Continental lithosphere thinning factors for a serpentinized mantle solution reach 1.0 at the western end of the profile, which implies the presence of exhumed mantle. The magma poor solution predicts continental lithosphere thinning factors of 0.9 for the same region.

3.2. RDAs corrected for Sediment Loading and Crustal Basement Thickness Variations along Lusigal 12

Sediment corrected RDAs and RDA_{CT} have been computed along the Lusigal 12 profile as shown in Figure 6(b) and show the same general trend, however, with varying magnitudes. The sediment corrected RDA ranges between -500m and -1500m in the west, implying that the presence of crust which is thinner than 7km or anomalous subsidence. At the western end of the profile, the RDA_{CT} ranges between -800m and -1000m, corresponding to either the presence of crust which is thinner than 7km, or the presence of exhumed mantle. Figure 6(c) shows the ΔRDA plot for Lusigal 12, which illustrates the sediment corrected RDA further corrected for crustal basement thickness variations. The ΔRDA ranges between zero and -500m implying that there is anomalous subsidence along Lusigal 12, which is in agreement with the anomalous subsidence predicted by RDA analysis along profile IAM9, the other profile in the Iberian Abyssal Plain.

3.3. Continental Lithosphere Thinning from Subsidence Analysis along Lusigal 12

Continental lithosphere thinning factors determined from subsidence analysis are shown in Figure 7(b); at the western end of the Lusigal 12 profile, continental lithosphere thinning factors from subsidence analysis are between 0.85 and 1.0, indicative of oceanic crust or possibly exhumed mantle. Sensitivities to the three magmatic solutions have been examined. Assuming a 'normal' magmatic solution, subsidence analysis predicts continental lithosphere thinning factors of 1.0 in the centre and western end of the profile, which for this magmatic assumption would indicate the presence of oceanic crust. The magma-starved solution with no serpentinization does not reach a continental lithosphere thinning factor of 1.0, except at the extreme western end of the profile. The solution assuming serpentinized mantle reaches thinning factors exceeding 0.95 for the western part of the profile. In section 5, we discuss the interpretation of these continental lithosphere thinning factors to determine COB location and crustal type.

4. OCT Structure along Profile ISE-01

4.1. Crustal Basement Thickness and Continental Lithosphere Thinning along ISE-01 from Gravity Anomaly Inversion

Gravity anomaly inversion has been applied in order to determine crustal basement thickness, Moho depth and continental lithosphere thinning along profile ISE-01. Sediment thicknesses (Figure 8(a)) used in the gravity anomaly inversion are from University of Texas Institute of Geophysics (UTIG) seismic database. Sensitivities to reference Moho depths have been examined within the gravity anomaly inversion along profile ISE-01, reference Moho depth sensitivities of 35km, 37.5km and 40km are shown in Figure 8(b). A reference Moho depth of 35km is too small and predicts a Moho which is too shallow and comes up into the sediments at the start of the profile, whereas both reference Moho depths of 37.5km and 40km predict more sensible Moho depths; calibration of the

451 reference Moho depth is therefore required. Zelt et al. (2003) uses first arrival seismic tomography
452 and reflection tomography to investigate the seismic velocity structure of the ISE-01 profile. They
453 show P-wave iso-velocity contours between 7kms^{-1} and 7.6kms^{-1}, but are not able to resolve the
454 expected higher seismic velocities consistent with rays sampling the mantle. Their seismic Moho
455 based on first arrival seismic tomography and reflection tomography typically fall within the 7kms^{-1}
456 and 7.6kms^{-1} range, suggesting that their seismic Moho is too shallow. Calibration of Moho depths
457 for the gravity anomaly inversion should only be done on unequivocal oceanic crust (or very well
458 seismically constrained Moho depths beneath continental crust). ODP wells along ISE-01 do not
459 observe oceanic crust, nor is there any well constrained seismic Moho, so calibration of the
460 reference Moho depth for ISE-01, using seismic Moho depths has not been possible. As a
461 consequence we have used the reference Moho depth of 41km for the gravity anomaly inversion
462 determined from profile IAM9.

463 Crustal cross section (C-C') along ISE-01 (Figure 8(c)) shows Moho depths from gravity anomaly
464 inversion using the reference Moho depth of 41km calibrated on line IAM9. The Moho depth from
465 gravity inversion is substantially deeper than the Moho determined by Zelt et al. (2003) from seismic
466 reflections. Sediment thicknesses used within the gravity anomaly inversion are derived from the
467 seismic pick of top basement from ISE-01 reflection data. We note however that the seismic
468 tomography from Zelt et al. (2003) shows upper crustal seismic velocities suggesting that there may
469 be several kilometres of pre-rift sediments beneath the seismic reflection top basement for both the
470 Galicia Interior Basin and Galicia Bank. Inclusion of a significant thickness of pre-rift sediments in the
471 gravity anomaly inversion would give a shallower Moho, closer to that proposed by Zelt et al. (2003).
472 Alternatively using a lighter crustal basement density would also result in a shallower Moho from the
473 gravity inversion. The P-wave iso-velocity contours of 7kms^{-1} and 7.6kms^{-1} from Zelt et al. (2003) are
474 also shown on Figure 8(c); the seismic tomography does not show seismic velocities typical of
475 normal mantle. The seismic reflection Moho of Zelt et al. (2003) plots between these iso-velocity

476 contours. We speculate that the reflection returns used by Zelt e al. (2003) to determine Moho
477 depth may be from the top of a lower crustal intrusive body rather than from the top of the mantle.
478 Whatever the cause of the difference between the gravity and seismic Moho depths under the
479 Galicia Interior Basin and Galicia Bank, the calibration of reference Moho depth in the oceanic
480 domain means that this problem as little effect on the gravity inversion results for the distal part of
481 the margin.

482 Figure 8(d) shows continental lithosphere thinning factor (γ) estimates from gravity anomaly
483 inversion for profile ISE-01 assuming a magma-starved model; a 'normal' magmatic solution and a
484 solution for serpentinized mantle. A 'normal' magmatic solution predicts continental lithosphere
485 thinning factors of 1.0 at the western end of the profile. A magma-starved solution, with no
486 serpentinization predicts continental lithosphere thinning factors that do not reach 1.0 anywhere. A
487 solution for serpentinized mantle shows continental lithosphere thinning factors reaching 1.0 at the
488 extreme western end of the profile.

489 ## 4.2. RDAs Corrected for Sediment Loading and Crustal Basement Thickness
490 ## Variations along ISE-01

491 At the western end of the ISE-01 profile, the sediment corrected RDA ranges between zero and -
492 800m (Figure 9(b)), which implies either the presence of crust, which is thinner than 7km or
493 anomalous subsidence. The RDA_{CT} ranges between zero and -1000m (Figure 9(b)), which
494 corresponds to the presence of crust which is thinner than 7km, or the presence of exhumed mantle.
495 The sediment corrected RDA and the RDA_{CT} along profile ISE-01 (Figure 9(b)) show the same general
496 trend. The sediment corrected RDA further corrected for variations in crustal basement thickness
497 (ΔRDA) (Figure 9(c)) is approximately zero implying that there is negligible anomalous subsidence or
498 uplift to the west of Galicia Bank.

4.3. Continental Lithosphere Thinning from Subsidence Analysis along ISE-01

Subsidence analysis using a 'normal' magmatic solution predicts continental lithosphere thinning factors of 1.0 at the western end of the profile (Figure 10(b)). The magma-starved solution with no serpentinization, nor the solution for serpentinized mantle, reach continental lithosphere thinning factors of 1.0; maximum values reached are 0.9.

5. Predicting OCT Structure and COB Location

The previous sections have shown the results from integrated quantitative analysis using gravity anomaly inversion, RDA and subsidence analysis, applied to IAM9 and Lusigal 12 in the Iberian Abyssal Plain and ISE-01 on Galicia Bank. The results from each of these techniques may be used to assist in understanding the transition from continental to oceanic crust; however, it is preferable that the results from each technique should to be examined together. For each of the three profiles considered, a composite analysis plot is used to summarize the results from gravity anomaly inversion, RDA and subsidence analysis, as shown in Figures 11, 12 and 13. The composite analysis plot consists of (i) a crustal cross section from gravity anomaly inversion, (ii) sediment corrected RDA and RDA_{CT} along profile and (iii) a comparison of the continental lithosphere thinning factors predicted from gravity anomaly inversion and subsidence analysis. The analysis of the composite plot allows for an informative interpretation of the OCT structure, COB location and crustal type to be made, when the crustal domains are clearly defined. Using ODP wells, located along the Lusigal 12 and ISE-01 profiles, we compare the predicted OCT structure and COB location determined from integrated quantitative analysis with that inferred from direct well observations.

Table 1 summarises the crustal types encountered along the western Iberian profiles and the consequent ranges of crustal basement thicknesses, continental lithosphere thinning factors and residual depth anomaly results predicted from the integrated analysis techniques that we would

522 expect to see in each of these domains. We use a crustal thickness of 10 km to mark the transition
523 from the necking zone to hyper-extended continental crust (consistent with Aslanian et al. (2009)).
524 The interpreted boundaries between each of these crustal types are based on these values (Table 1)
525 and correspond to changes in crustal basement thickness from gravity anomaly inversion, variations
526 in the RDA signal from the sediment corrected RDA and RDA_{CT}, and changes in continental
527 lithosphere thinning factors derived from subsidence analysis and gravity anomaly inversion. Whilst
528 we use the values in Table 1 for the results from each analytical technique to identify the various
529 crustal domain along profile and locate the boundaries between these different crustal types, when
530 considering all the techniques together there are discrepancies between the predicted locations of
531 these boundaries. The transitional nature of these boundaries may in part explain these
532 discrepancies. In our interpretation, we first picked the boundaries using the results from each
533 individual technique and then considered all the techniques together so that our boundaries reflect
534 the 'best-fit' from the integrated approach.

535

536 ## 5.1. IAM9

537 The composite analysis plot for profile IAM9 in the Iberian Abyssal Plain (Figure 11) is interpreted as
538 showing three distinct crustal types: oceanic crust (zone A), serpentinized exhumed mantle (zone B)
539 and continental crust which can be further subdivided into hyper-extended continental crust (zone
540 C), the crustal necking zone (zone D), and proximal continental crust (zone E). We have examined
541 the relationship between our interpretations of the boundaries between these three crustal types to
542 those proposed in the literature, in particular the J anomaly. The J anomaly is a structural ridge or
543 step in the oceanic basement that lies beneath the J magnetic anomaly (Tucholke and Ludwig, 1982).
544 Whilst the J anomaly and the interfaces between the crustal zones are shown as sharp lines, in
545 reality they are likely to be transitional boundaries. The J anomaly is identified at approximately

25km distance along the IAM9 profile (Figure 11(a)) (Bronner et al., 2011; Dean et al., 2000; Whitmarsh et al., 2001), and corresponds to inflection points in Moho depth, RDA and continental lithosphere thinning factors, determined assuming a magma-starved solution, and is west of our interpreted COB.

The discussions below refer to Figure 11, unless otherwise stated.

Zone A – oceanic crust

In zone A, the crustal basement thicknesses from gravity anomaly inversion are between 6km and 7km. The negative sediment corrected RDA is indicative of crust which is thinner than 7km or anomalous subsidence, whilst the negative RDA_{CT} (shown in Figure 3(f)) corresponds to the presence of thin crust derived from gravity anomaly inversion. The continental lithosphere thinning factors in zone A derived from gravity anomaly inversion and subsidence analysis using a 'normal' magmatic solution are 1.0 (shown in Figure 2(d) and 4(e)) , implying the presence of oceanic crust.

If a magma-starved or a serpentinized mantle solution is assumed, the continental lithosphere thinning factors do not reach 1.0 from both gravity anomaly inversion and subsidence analysis, which implies thin continental crust. In zone A, a 'normal' magmatic solution is preferred as it produces high thinning factors of 1.0 which, together with crustal basement thicknesses between 6 and 7km, we interpret as indicators for the presence of oceanic crust, consistent with the literature.

The interface between zones A and B corresponds to the boundary between oceanic crust and serpentinized exhumed mantle and is located by changes in Moho depth, RDAs and continental lithosphere thinning factors determined assuming magma-starved or a serpentinized mantle solution.

Zone B – exhumed mantle

In zone B, the crustal basement thicknesses decrease from 7km in the west to approximately 3km at the eastern end of the zone. These very low values of crustal thicknesses are apparent crustal thicknesses derived from the mass deficiency of serpentinized exhumed mantle with respect to unserpentinized mantle below (Appendix A). Thicknesses of 3km or less are indicative of the presence of serpentinized exhumed mantle; the very low crustal thicknesses derived from gravity anomaly inversion are not interpreted as very thin continental or oceanic crust. Sediment corrected RDA and RDA_{CT} (shown in Figure 3(f)) are both negative in zone B, corresponding to the presence of crust which is thinner than 7km or anomalous subsidence. The continental lithosphere thinning factors from gravity anomaly inversion and subsidence analysis assuming a serpentinized mantle solution are 1.0 consistent with the presence of serpentinized exhumed mantle.

The interface between zones B and C corresponds to the boundary between thinned continental crust and exhumed mantle and is located by the inflection points in Moho depth, RDAs and continental lithosphere thinning factors determined assuming a solution for serpentinized mantle. Gravity anomaly inversion, RDA and subsidence analysis results show that the OCT along IAM9 is relatively narrow, with the distance between the COB and the proximal start of the necking zone measuring less than 100km.

Zones C, D and E- continental crust

In zones C, D and E, the crustal basement thicknesses increase gradually to approximately 35km at the eastern end of the profile, although the poor resolution of sediment thickness in this region may result in an overestimate of Moho depth. Both the sediment corrected RDA and RDA_{CT} (shown in Figure 3(f)) increase eastwards. The continental lithosphere thinning factors from gravity anomaly inversion and subsidence analysis show a corresponding eastwards decrease. We tentatively interpret the composite analysis plot (Figure 11) to show the location of hyper-extended continental crust and the crustal necking zone. The combined width of the hyper-extended continental crust

and necking zone appears to be very narrow and it is difficult to place the transition from one to the other.

Figure 11(e) shows a comparison of our interpretations of the crustal types along the IAM9 profile with those interpreted by Dean et al. (2000) and Bronner et al. (2001). Our interpreted location of the boundary between oceanic crust and exhumed mantle is similar to that interpreted by Dean et al. (2000) although we place the boundary between continental crust and exhumed mantle slightly more landward. Although the interpreted boundary between oceanic crust and exhumed mantle from Bronner et al. (2001) is significantly more distal than our interpreted boundary, it does correspond to slight changes in crustal basement thickness, RDAs and continental lithosphere thinning factors determined assuming magma-starved or a serpentinized mantle solution.

5.2. Lusigal 12

The composite analysis plot for the Lusigal 12 profile in the Iberian Abyssal Plain (Figure 12) is interpreted as showing two distinct crustal types: serpentinized exhumed mantle (zone B), and thinned continental crust, which can be further subdivided into hyper-extended continental crust (zone C) and the crustal necking zone (zone D). No unequivocal oceanic crust of 'normal' thickness (corresponding to zone A on the IAM9 profile) is evident on Lusigal 12. The interpretation of these zones of serpentinized exhumed mantle and thinned continental crust, and their boundary, along Lusigal 12 have been validated against ODP well data and other previous studies (e.g. Péron-Pinvidic & Manatschal (2009) and Sutra & Manatschal (2012)).

The discussions below refer to Figure 12, unless otherwise stated.

Zone B – exhumed mantle

In zone B, the crustal basement thicknesses predicted, from gravity anomaly inversion, range between 2km and 4km. These very low values of crustal thickness are interpreted as being indicative of serpentinized exhumed mantle (see earlier discussion for IAM9). Both the sediment corrected RDA and RDA_{CT} (Figure 6(b)) are negative in this region. The sediment corrected RDA is negative between -500m and -1500m, implying that the crust in this region is substantially less than 7km thick or that there is anomalous subsidence. The continental lithosphere thinning factors for the serpentinized mantle solution from the gravity anomaly inversion show a value of 1.0 in this region consistent with the presence of serpentinized exhumed mantle; whilst from subsidence analysis they range between 0.95 and 1.0. Both the gravity anomaly inversion and subsidence analysis thinning factors show a marked inflection at the inner boundary of zone B. For zone B, a serpentinized mantle solution is preferred, as it predicts high thinning factors without the requirement of magmatic addition (and the formation of oceanic crust).

The COB, corresponding to the interface between zones B and C, is located by the inflection points in Moho depth, RDAs and continental lithosphere thinning factors determined for solutions assuming both magma-starved and serpentinized mantle. Gravity anomaly inversion, RDA and subsidence analysis results show that the OCT along Lusigal 12 is wider than that for IAM9, with the distance between the COB and the proximal start of the necking zone measuring more than 150km.

Zones C and D - continental crust

In zones C and D, crustal thicknesses predicted from gravity anomaly inversion increase eastwards towards the continent, as do the sediment corrected RDAs and RDA_{CT} (Figure 6(b)), whilst the continental lithosphere thinning factors from gravity anomaly inversion and subsidence analysis decrease. This is indicative of zone C and D corresponding to thinned continental crust. A magma-starved solution for the prediction of RDA and continental lithosphere thinning factors is preferred for this zone. We identify the boundary between hyper-extended crust (zone C) and the crustal

necking zone (zone D) using a combination of changes in crustal basement thickness, variations in RDA and changes in continental lithosphere thinning factors.

We compare our interpretation of the crustal types along the Lusigal 12 profile with those interpreted by Péron-Pinvidic & Manatschal (2009) and Sutra & Manatschal (2012) in Figure 12(e). Our interpretation of the boundary between oceanic crust and exhumed mantle compares well with both.

Comparison with ODP well observations

Observations from the ODP drill logs (897, 899, 901, 1065, 1067, 1068, 1069 and 1070) along Lusigal 12 are summarised in Figure 12(a) and in Table 1. Our interpretation of crustal types from the composite analysis plot (Figure 12) and summarized in Figure 12(e) is consistent with the ODP well observations. ODP well logs (1070, 899 and 897), in zone B, show the presence of serpentinized peridotite, serpentinite, serpentinized plagioclase, breccia and mantle, which are in agreement with our interpretation of the presence of exhumed mantle from the composite analysis plot. The ODP wells (1069, 1068, 1067, 1065 and 901), in zone C, indicate the presence of pre-tectonic outer-shelf carbonates, which suggest the occurrence of upper continental crust, which is in agreement with our interpretations of the composite analysis plot.

5.3. ISE-01

Interpretation of the composite analysis plots of profile ISE-01 on Galicia Bank (Figure 13) suggests that there are two crustal types along the profile; exhumed mantle (zone B) and continental crust, which can be subdivided into hyper-extended crust (zone C), the crustal necking zone (zone D) and proximal continental crust (zone E). These interpretations, based on gravity anomaly inversion, RDA and subsidence analysis, are consistent with ODP well data on profile ISE-01. As with Lusigal 12, no

660 oceanic crust of 'normal' thickness (corresponding to zone A on the IAM9 profile) is evident on ISE-
661 01.

662 The discussions below refer to Figure 13, unless otherwise stated.

663 *Zone B – exhumed mantle*

664 In zone B at the western end of the profile, crustal basement thicknesses, from gravity anomaly
665 inversion, range between 4km and 5km and RDA analysis shows negative sediment corrected RDAs
666 and RDA_{CT} (Figure 9(b)) in this region. The low values of crustal thickness from gravity anomaly
667 inversion in this region (and the resulting RDA_{CT} ranging between zero and -1000m) are interpreted
668 as being indicative of serpentinized exhumed mantle (see earlier discussion for IAM9). The sediment
669 corrected RDA ranges between zero and -800m, which implies either the presence of crust, which is
670 thinner than 7km, or anomalous subsidence. In zone B, if a serpentinized mantle solution is
671 assumed, the continental lithosphere thinning factors reach 1.0 from gravity anomaly inversion and
672 exceed 0.9 from subsidence analysis, which we interpret as indicating the start of serpentinized
673 exhumed mantle.

674 The COB for profile ISE-01 is interpreted as being at the interface between zones B and C and
675 corresponds to inflection points in Moho depth, RDA and continental lithosphere thinning factors
676 determined assuming the serpentinized mantle solution. In contrast to profiles IAM9 and Lusigal 12,
677 ISE-01 shows a very broad region between the proximal start of the necking zone and COB; the
678 distance separating these is of the order 250km.

679 *Zones C, D and E - continental crust*

680 In zones C, D and E, the crustal basement thickens and the RDA values increase eastwards towards
681 the continent. These and the corresponding decrease in continental lithosphere thinning factors
682 imply the presence of thinned continental crust in these zones. Continental lithosphere thinning

683 factors predicted from gravity anomaly inversion are in good agreement with those predicted from
684 subsidence analysis.

685 In Figure 13(e) we compare our interpretation of the location of crustal types with those of Sutra &
686 Manatschal (2012) and Dean et al. (2015). The three interpretations are in close agreement. The
687 'western extension 2 (WE2)' seismic reflection line of Dean et al. (2015) lies close and parallel to the
688 ISE-01 profile and supports the existence of hyper-extended crust within our interpreted zone C.
689 Zelt et al. (2003) do not interpret their seismic cross-section in terms of crustal types.

690 *Comparison with ODP well observations*

691 Observations from the ODP drill logs (637, 638, 639 and 640) along profile ISE-01 are summarised in
692 Figure (13(a)) and Table 2 and have been compared to our interpretations made from the integrated
693 quantitative analysis shown on the composite analysis plot for profile ISE-01. Our interpretations
694 are consistent with the ODP well data. The ODP well 637, in zone B, shows the presence of
695 serpentinized peridotite, whilst ODP well 639, in zone C, shows the presence of continental
696 basement. The interpretation of the composite analysis plot for profile ISE-01 is consistent with the
697 ODP observations at both of these wells. ODP well logs 638 and 640, in zone C, are much shallower
698 only showing the presence of syn-rift sediments.

699 ## 6. Conclusion

700 The gravity anomaly inversion, RDA and subsidence analysis techniques are of global applicability
701 and may be used on many deep-water frontier rifted continental margins, in order to assist in
702 understanding the large scale distribution of thinned continental crust and lithosphere, the start of
703 unequivocal oceanic crust and hence determine the structure of the OCT, COB location and
704 magmatic type. Testing of these techniques has been carried out on the west Iberian rifted
705 continental margin, as this is one of the best-studied margins worldwide, due to the abundance of

ODP well data. Integrated quantitative analysis of the west Iberian seismic profiles (IAM9, Lusigal 12 and ISE-01) has enabled further geological interpretations to be made of the crustal structure and distribution, which are validated using ODP well data, and where ODP well data are ambiguous, predictions have been made. Integrated quantitative analysis of the west Iberian seismic profiles show the crustal structure and the distribution of thinned continental crust, exhumed mantle and the start of unequivocal oceanic crust (where present) along the margin. The integrated approach, which considers the gravity anomaly inversion, RDA and subsidence analysis techniques together, has enabled a less subjective geological interpretation of the OCT structure along the seismic profiles and a more accurate prediction of the COB location to be made. Predicted distances between the COB and the proximal start of the necking zone for the west Iberian margin range between 100km and 250km, with the greatest distances predicted for Galicia Bank. Our interpretation of crustal types based on our composite analysis has been compared with that of previous workers and is generally consistent.

An accurate identification of the crustal structure and the distribution of continental and oceanic crust remains crucial in order to fully understand the evolution of the west Iberian rifted continental margin, with fundamental implications for building a better geodynamic history and plate tectonic reconstruction model, and for the evolution of petroleum systems. We suggest that the integrated quantitative analysis techniques described in this paper provide useful assistance to high receiver-density wide-angle seismology and deep-long offset reflection seismology for the determination of ocean-continent transition structure, continent-ocean boundary location and crustal type at rifted continental margins.

7. Appendix A - The Mass Deficiency of Serpentinised Exhumed Mantle

Seismic refraction data on the exhumed serpentinised mantle of the IAM9 seismic profile have been interpreted by Cole et al. (2002) and Skelton et al. (2005) to determine the variation in the degree of serpentinization with depth. Their results (Figure A1(a)) summarised by Cooper (2010) suggest that serpentinization approaches 100% in the top 1.5- 2.0km below top basement, but then attenuates with depth reaching approximately 5% serpentinization at 5km depth. Cooper (2010), following the scheme of Shelton et al. (2005), determined the variation of density with depth (Figure A1(b)) for the serpentinized mantle of IAM9 as a function of magnetite content; his preferred density-depth model uses 4.5% magnetite.

The integrated mass-deficiency of serpentinized mantle with respect to un-serpentinized mantle assuming 4.5% magnetite content is shown in Figure A1(c) as a function of depth. The plot shows that the majority of the mass deficiency of serpentinized mantle derives from the topmost 2-3km of serpentinized mantle, and that the mass deficiency reaches a constant asymptotic maximum (the degree of serpentinization tends to zero as depth increases). For comparison the mass deficiency of crustal basement with a density of 2850kgm^{-3} with respect to mantle (assumed density = 3300kgm^{-3}) is shown as a function of the depth to the base of crustal basement (i.e. crustal basement thickness). The plot shows that the mass deficiency of serpentinized exhumed mantle is equivalent to the mass deficiency of crustal basement with a thickness of 3.1km.

The density of serpentinized mantle is important for both the determination of Moho depth from gravity anomaly inversion, and also for subsidence analysis to determine lithosphere stretching and thinning factors. The analysis based on IAM9 summarised above suggests that the gravitational and isostatic signals of serpentinized exhumed mantle are equivalent to a crustal basement thickness of approximately 3km.

754 # 8. References

755 Alvey, A., Gaina, C., Kusznir, N. J., and Torsvik, T. H., 2008, Integrated crustal thickness mapping and
756 plate reconstructions for the high Arctic: Earth and Planetary Science Letters, v. 274, no. 3-4,
757 p. 310-321.
758 Amante, C., and Eakins, B. W., 2009, ETOPO1 1 Arc-Minute Global Relief Model: Procedures, Data
759 Sources and Analysis: NOAA Technical Memorandum NESDIS NGDC-24, p. 19.
760 Aslanian, D., Moulin, M., Olivet, J.-L., Unternehr, P., Matias, L., Bache, F., Rabineau, M., Nouzé, H.,
761 Klingelheofer, F., Contrucci, I., and Labails, C., 2009, Brazilian and African passive margins of
762 the Central Segment of the South Atlantic Ocean: Kinematic constraints: Tectonophysics, v.
763 468, no. 1–4, p. 98-112.
764 Autin, J., Leroy, S., Beslier, M.-O., d'Acremont, E., Razin, P., Ribodetti, A., Bellahsen, N., Robin, C., and
765 Al Toubi, K., 2010, Continental break-up history of a deep magma-poor margin based on
766 seismic reflection data (northeastern Gulf of Aden margin, offshore Oman): Geophysical
767 Journal International, v. 180, no. 2, p. 501-519.
768 Boillot, G., Grimaud, S., Mauffret, A., Mougenot, D., Kornprobst, J., Mergoil-Daniel, J., and Torrent,
769 G., 1980, Ocean-continent boundary off the Iberian margin: A serpentinite diapir west of the
770 Galicia Bank: Earth and Planetary Science Letters, v. 48, no. 1, p. 23-34.
771 Boillot, G., Recq, M., Winterer, E. L., Meyer, A. W., Applegate, J., Baltuck, M., Bergen, J. A., Comas,
772 M. C., Davies, T. A., Dunham, K., Evans, C. A., Girardeau, J., Goldberg, G., Haggerty, J., Jansa,
773 L. F., Johnson, J. A., Kasahara, J., Loreau, J. P., Luna-Sierra, E., Moullade, M., Ogg, J., Sarti, M.,
774 Thurow, J., and Williamson, M., 1987, Tectonic denudation of the upper mantle along
775 passive margins: a model based on drilling results (ODP leg 103, western Galicia margin,
776 Spain): Tectonophysics, v. 132, no. 4, p. 335-342.
777 Bronner, A., Sauter, D., Manatschal, G., Peron-Pinvidic, G., and Munschy, M., 2011, Magmatic
778 breakup as an explanation for magnetic anomalies at magma-poor rifted margins, Nature
779 Geoscience, Volume 4, Nature Publishing Group, a division of Macmillan Publishers Limited.
780 All Rights Reserved., p. 5.
781 Carlson, R. L., and Herrick, C. N., 1990, Densities and porosities in the oceanic crust and their
782 variations with depth and age: Journal of Geophysical Research: Solid Earth, v. 95, no. B6, p.
783 9153-9170.
784 Chappell, A. R., and Kusznir, N. J., 2008, Three-dimensional gravity inversion for Moho depth at rifted
785 continental margins incorporating a lithosphere thermal gravity anomaly correction:
786 Geophysical Journal International, v. 174, no. 1, p. 1-13.
787 Chian, D., Louden, K. E., Minshull, T. A., and Whitmarsh, R. B., 1999, Deep structure of the ocean-
788 continent transition in the southern Iberia Abyssal Plain from seismic refraction profiles:
789 Ocean Drilling Program (Legs 149 and 173) transect: Journal of Geophysical Research: Solid
790 Earth, v. 104, no. B4, p. 7443-7462.
791 Christensen, N. I., and Mooney, W. D., 1995, Seismic velocity structure and composition of the
792 continental crust: A global view: Journal of Geophysical Research: Solid Earth, v. 100, no. B6,
793 p. 9761-9788.
794 Coffin, M. F., and Eldholm, O., 1994, Large igneous provinces: Crustal structure, dimensions, and
795 external consequences: Reviews of Geophysics, v. 32, no. 1, p. 1-36.
796 Cole, P. B., Minshull, T. A., and Whitmarsh, R. B., 2002, Azimuthal seismic anisotropy in a zone of
797 exhumed continental mantle, West Iberia margin: Geophysical Journal International, v. 151,
798 no. 2, p. 517-533.
799 Contrucci, I., Matias, L., Moulin, M., Géli, L., Klingelhofer, F., Nouzé, H., Aslanian, D., Olivet, J.-L.,
800 Réhault, J.-P., and Sibuet, J.-C., 2004, Deep structure of the West African continental margin
801 (Congo, Zaïre, Angola), between 5°S and 8°S, from reflection/refraction seismics and gravity
802 data: Geophysical Journal International, v. 158, no. 2, p. 529-553.

803 Cooper, C., 2010, Anomalous Bathymetry and Mass Heterogeneity at the Conjugate Iberia and
804 Newfoundland Rifted Margins [PhD: University of Liverpool, 260 p.
805 Cowie, L., and Kusznir, N., 2012, Mapping crustal thickness and oceanic lithosphere distribution in
806 the Eastern Mediterranean using gravity inversion: Petroleum Geoscience, v. 18, no. 4, p.
807 373-380.
808 Crosby, A. G., and McKenzie, D., 2009, An analysis of young ocean depth, gravity and global residual
809 topography: Geophysical Journal International, v. 178, no. 3, p. 1198-1219.
810 Crosby, A. G., McKenzie, D., and Sclater, J. G., 2006, The relationship between depth, age and gravity
811 in the oceans: Geophysical Journal International, v. 166, no. 2, p. 553-573.
812 D'Acremont, E., Leroy, S., Beslier, M.-O., Bellahsen, N., Fournier, M., Robin, C., Maia, M., and Gente,
813 P., 2005, Structure and evolution of the eastern Gulf of Aden conjugate margins from
814 seismic reflection data: Geophysical Journal International, v. 160, no. 3, p. 869-890.
815 Dean, S. M., Minshull, T. A., Whitmarsh, R. B., and Louden, K. E., 2000, Deep structure of the ocean-
816 continent transition in the southern Iberia Abyssal Plain from seismic refraction profiles: The
817 IAM-9 transect at 40°20'N: Journal of Geophysical Research: Solid Earth, v. 105, no. B3, p.
818 5859-5885.
819 Discovery 215 Working, G., Minshull, T. A., Dean, S. M., Whitmarsh, R. B., Russell, S. M., Louden, K.
820 E., and Chian, D., 1998, Deep structure in the vicinity of the ocean-continent transition zone
821 under the southern Iberia Abyssal Plain: Geology, v. 26, no. 8, p. 743-746.
822 Franke, D., 2013, Rifting, lithosphere breakup and volcanism: Comparison of magma-poor and
823 volcanic rifted margins: Marine and Petroleum Geology, v. 43, no. 0, p. 63-87.
824 Greenhalgh, E. E., and Kusznir, N. J., 2007, Evidence for thin oceanic crust on the extinct Aegir Ridge,
825 Norwegian Basin, NE Atlantic derived from satellite gravity inversion: Geophysical Research
826 Letters, v. 34, no. 6, p. L06305.
827 Henning, A. T., Sawyer, D. S., and Templeton, D. C., 2004, Exhumed upper mantle within the ocean-
828 continent transition on the northern West Iberia margin: Evidence from prestack depth
829 migration and total tectonic subsidence analyses: Journal of Geophysical Research: Solid
830 Earth, v. 109, no. B5, p. n/a-n/a.
831 Hinz, K., 1981, A hypothesis on terrestrial catastrophes: wedges of very thick oceanward dipping
832 layers beneath passive continental margins - their origin and paleoenvironmental
833 significance. : Geologisches Jahrbuch Reihe E, p. 3-28.
834 Hopper, J. R., Funck, T., Tucholke, B. E., Larsen, H. C., Holbrook, W. S., Louden, K. E., Shillington, D.,
835 and Lau, H., 2004, Continental breakup and the onset of ultraslow seafloor spreading off
836 Flemish Cap on the Newfoundland rifted margin: Geology, v. 32, no. 1, p. 93-96.
837 Jordan, T. H., and Anderson, D. L., 1974, Earth Structure from Free Oscillations and Travel Times*:
838 Geophysical Journal of the Royal Astronomical Society, v. 36, no. 2, p. 411-459.
839 Kusznir, N., and Karner, G., 1985, Dependence of the flexural rigidity of the continental lithosphere
840 on rheology and temperature: Nature, v. 316, no. 6024, p. 138-142.
841 Kusznir, N. J., Roberts, A. M., and Morley, C. K., 1995, Forward and reverse modelling of rift basin
842 formation: Geological Society, London, Special Publications, v. 80, no. 1, p. 33-56.
843 Manatschal, G., 2004, New models for evolution of magma-poor rifted margins based on a review of
844 data and concepts from West Iberia and the Alps: International Journal of Earth Sciences, v.
845 93, no. 3.
846 Manatschal, G., Froitzheim, N., Rubenach, M., and Turrin, B. D., 2001, The role of detachment
847 faulting in the formation of an ocean-continent transition: insights from the Iberia Abyssal
848 Plain: Geological Society, London, Special Publications, v. 187, no. 1, p. 405-428.
849 Manatschal, G., Sutra, E., and Péron-Pinvidic, G., The lesson from the Iberia-Newfoundland rifted
850 margins: how applicable is it to other rifted margins?, *in* Proceedings 2nd Central & North
851 Atlantic Conjugate Margins: Rediscovering the Atlantic, New Insights, New winds for an old
852 sea2010, Volume 2, p. 27 - 37.

McKenzie, D., 1978, Some Remarks on the Development of Sedimentary Basins Earth and Planetary Science Letters, v. 40, p. 25-32.
Müller, R. D., Roest, W. R., Royer, J.-Y., Gahagan, L. M., and Sclater, J. G., 1997, Digital isochrons of the world's ocean floor: Journal of Geophysical Research, v. 102, no. B2, p. 3211-3214.
Müller, R. D., Sdrolias, M., Gaina, C., Steinberger, B., and Heine, C., 2008, Long-Term Sea-Level Fluctuations Driven by Ocean Basin Dynamics: Science, v. 319, no. 5868, p. 1357-1362.
Parker, R. L., 1972, The Rapid Calculation of Potential Anomalies: Geophysical Journal of the Royal Astronomical Society, v. 31, no. 4, p. 447-455.
Parsons, B., and Sclater, J. G., 1977, An Analysis of the Variation of Ocean Floor Bathymetry and Heat Flow with Age: Journal of Geophysical Research, v. 82, no. 5, p. 803-827.
Pérez-Gussinyé, M., 2012, A tectonic model for hyperextension at magma-poor rifted margins: an example from the West Iberia–Newfoundland conjugate margins: Geological Society, London, Special Publications, v. 369.
Péron-Pinvidic, G., Manatschal, G., Minshull, T. A., and Sawyer, D. S., 2007, Tectonosedimentary evolution of the deep Iberia-Newfoundland margins: Evidence for a complex breakup history: Tectonics, v. 26, no. 2, p. TC2011.
Pickup, S. L. B., Whitmarsh, R. B., Fowler, C. M. R., and Reston, T. J., 1996, Insight into the nature of the ocean-continent transition off West Iberia from a deep multichannel seismic reflection profile: Geology, v. 24, no. 12, p. 1079-1082.
Reston, T. J., 2009, The structure, evolution and symmetry of the magma-poor rifted margins of the North and Central Atlantic: A synthesis: Tectonophysics, v. 468, no. 1–4, p. 6-27.
Roberts, A. M., Kusznir, N. J., Corfield, R. I., Thompson, M., and Woodfine, R., 2013, Integrated tectonic basin modelling as an aid to understanding deep-water rifted continental margin structure and location: Petroleum Geoscience, v. 19, no. 1, p. 65-88.
Roberts, A. M., Kusznir, N. J., Yielding, G., and Styles, P., 1998, 2D flexural backstripping of extensional basins; the need for a sideways glance: Petroleum Geoscience, v. 4, no. 4, p. 327-338.
Russell, S. M., and Whitmarsh, R. B., 2003, Magmatism at the west Iberia non-volcanic rifted continental margin: evidence from analyses of magnetic anomalies: Geophysical Journal International, v. 154, no. 3, p. 706-730.
Sandwell, D. T., and Smith, W. H. F., 2009, Global marine gravity from retracked Geosat and ERS-1 altimetry: Ridge segmentation versus spreading rate: Journal of Geophysical Research, v. 114, no. B1, p. B01411.
Sawyer, D. S., Whitmarsh, R. B., Klaus, A., and et al., 1994, Proceedings of the ODP, Initial Reports, 149: College Station, TX (Ocean Drilling Program).
Sclater, J. G., and Christie, P. A. F., 1980, Continental stretching: An explanation of the Post-Mid-Cretaceous subsidence of the central North Sea Basin: Journal of Geophysical Research: Solid Earth, v. 85, no. B7, p. 3711-3739.
Skelton, A., Whitmarsh, R., Arghe, F., Crill, P., and Koyi, H., 2005, Constraining the rate and extent of mantle serpentinization from seismic and petrological data: implications for chemosynthesis and tectonic processes: Geofluids, v. 5, no. 3, p. 153-164.
Stein, C. A., and Stein, S., 1992, A model for the global variation in oceanic depth and heat flow with lithospheric age: Nature, v. 359, no. 6391, p. 123-129.
Sutra, E., and Manatschal, G., 2012, How does the continental crust thin in a hyperextended rifted margin? Insights from the Iberia margin: Geology, v. 40, no. 2, p. 139-142.
Sutra, E., Manatschal, G., Mohn, G., and Unternehr, P., 2013, Quantification and restoration of extensional deformation along the Western Iberia and Newfoundland rifted margins: Geochemistry, Geophysics, Geosystems, v. 14, no. 8, p. 2575-2597.
Tucholke, B. E., and Ludwig, W. J., 1982, Structure and origin of the J Anomaly Ridge, western North Atlantic Ocean: Journal of Geophysical Research: Solid Earth, v. 87, no. B11, p. 9389-9407.

903 Tucholke, B. E., Sawyer, D. S., and Sibuet, J. C., 2007, Breakup of the Newfoundland–Iberia rift:
904 Geological Society, London, Special Publications, v. 282, no. 1, p. 9-46.
905 Unternehr, P., Péron-Pinvidic, G., Manatschal, G., and Sutra, E., 2010, Hyper-extended crust in the
906 South Atlantic: in search of a model: Petroleum Geoscience, v. 16, no. 3, p. 207-215.
907 White, R. S., McKenzie, D., and O'Nions, R. K., 1992, Oceanic Crustal Thickness From Seismic
908 Measurements and Rare Earth Element Inversions: Journal of Geophysical Research, v. 97,
909 no. B13, p. 19683-19715.
910 White, R. S., Smith, L. K., Roberts, A. W., Christie, P. A. F., and Kusznir, N. J., 2008, Lower-crustal
911 intrusion on the North Atlantic continental margin: Nature, v. 452, no. 7186, p. 460 - 464.
912 Whitmarsh, R. B., Beslier, M. O., P.J., W., and et al., 1998, Proceedings of the ODP, Initial Reports,
913 173, College Station, TX (Ocean Drilling Program).
914 Whitmarsh, R. B., and Miles, P. R., 1995, Models of the development of the West Iberia rifted
915 continental margin at 40°30'N deduced from surface and deep-tow magnetic anomalies:
916 Journal of Geophysical Research: Solid Earth, v. 100, no. B3, p. 3789-3806.
917 Whitmarsh, R. B., Minshull, T. A., Russell, S. M., Dean, S. M., Louden, K. E., and Chian, D., 2001, The
918 role of syn-rift magmatism in the rift-to-drift evolution of the West Iberia continental
919 margin: geophysical observations: Geological Society, London, Special Publications, v. 187,
920 no. 1, p. 107-124.
921 Whitmarsh, R. B., and Sawyer, D. S., 1996, The ocean-continent transition beneath the Iberia Abyssal
922 Plain and continental rifting to seafloor spreading processes, *in* Whitmarsh, R. B., Sawyer, D.
923 S., Klaus, A., and Masson, D. G., eds., Proceedings of the Ocean Drilling Program, Scientific
924 Results 149: College Station, TX, p. 713 - 733.
925 Wilson, J. T., 1966, Did the Atlantic Close and then Re-Open?: Nature, v. 211, no. 5050, p. 676 - 681.
926 Zalán, P. V., Severino, M. C. G., Rigoti, C., Magnavita, L. P., Oliveira, J. A. B., and Viana, A. R., 2011, An
927 entirely new 3D-view of the crustal and mantle structure of a ruptured South Atlantic
928 passive margin – Santos, Campos and Espírito Santo Basins, Brazil (Expanded Abstract):
929 AAPG Annual Convention & Exhibition Abstracts Volume CDROM,Paper 986156.
930 .
931 Zelt, C. A., Sain, K., Naumenko, J. V., and Sawyer, D. S., 2003, Assessment of crustal velocity models
932 using seismic refraction and reflection tomography: Geophysical Journal International, v.
933 153, no. 3, p. 609-626.
934
935
936
937
938
939
940
941
942
943

944 **Tables:**

	Crustal Thickness (km)	Continental Lithosphere Thinning Factors (from Gravity Inversion & Subsidence Analysis)			Residual Depth Anomaly (m) *Assuming no mantle dynamic topography effects for sediment corrected RDA	
		Assuming Normal Magmatic	Assuming Magma Starved	Assuming Serpentinised Mantle	*RDA_{SC}	RDA_{CT}
Oceanic Crust (normal thickness)	7	1.0	0.8	0.9	Zero	Zero
Oceanic Crust (thin crust to magma poor)	0 to < 7	1.0	0.8 to 1	0.9 to 1.0	Negative	Negative
Serpentinised Exhumed Mantle	0 to 3	1.0	0.9	1.0	Negative	Negative
Hyper-extended Continental Crust	5 to 10	0.7 - 1.0	0.7 - 0.85	0.7 - 0.95	Negative to slightly positive	Negative to slightly positive
Continental Crust (within necking zone)	10 to 25	0.3 - 0.7	0.3 - 0.7	0.3 - 0.7	Slightly positive to very positive	Slightly positive to very positive
Continental Crust (inboard of necking zone)	25 +	0.0 - 0.3	0.0 - 0.3	0.0 - 0.3	Very positive	Very positive

945
946 **Table 1 –** Summary of crustal types encountered along the western Iberian profiles and the
947 consequent ranges of crustal basement thicknesses, continental lithosphere thinning factors and
948 residual depth anomaly results predicted from the integrated analysis techniques.
949 ➔ **Position in Main text:** Close to the table call. In Section 5.

ODP Well	Description
1070	Serpentinized peridotite
897	Serpentinized mantle
899	Serpentinized breccia
1069	Carbonates, upper crust
1068	Serpentinized peridotite (overlain by polymict breccias)
1067	Amphibolite, Minor Tonalite, Meta-gabbros
1065	Pre-tectonic sediments (carbonates) over upper crust
901	Pre-tectonic sediments (carbonates) over upper crust

Table 2 – ODP well observations along Lusigal 12 (Boillot et al., 1987; Sawyer et al., 1994; Tucholke et al., 2007; Whitmarsh et al., 1998; Whitmarsh and Sawyer, 1996).

➔ **Position in Main text:** Close to the table call. In Section 5.2 Lusigal 12, subheading "Comparison with ODP well observations".

ODP Well	Description
637	Serpentinized peridotite
640	Syn-rift sediments
638	Syn-rift sediments
639	Continental basement

Table 3 – ODP well observations along ISE-01 (Boillot et al., 1987; Sawyer et al., 1994; Tucholke et al., 2007; Whitmarsh et al., 1998; Whitmarsh and Sawyer, 1996).

➔ **Position in Main text:** Close to the table call. In Section 5.3 ISE-01, subheading "Comparison with ODP well observations".

1007

1008

1009

1010

1011

1012

1013

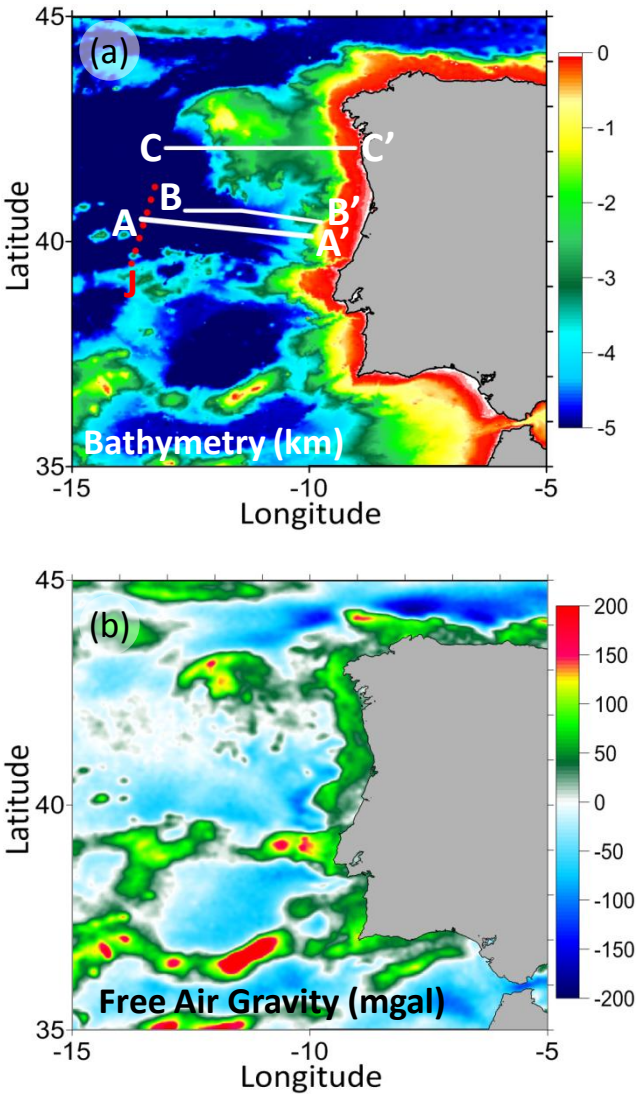

Figure 1 - Data used in the gravity anomaly inversion, RDA and subsidence analysis for the Iberian Abyssal Plain and Galicia Bank. (a) Bathymetry (km) (Amante and Eakins 2009). Locations of profiles IAM9 (A-A'), Lusigal 12 (with the TGS extension) (B-B') and ISE-01 (C-C') are indicated. The red dashed line indicates the location of the J anomaly (Bronner et al., 2011; Dean et al., 2000; Whitmarsh et al., 2001). (b) Free air gravity (mgal) (Sandwell and Smith 2009).

Figure 2
Cowie, Kusznir & Manatschal 2015

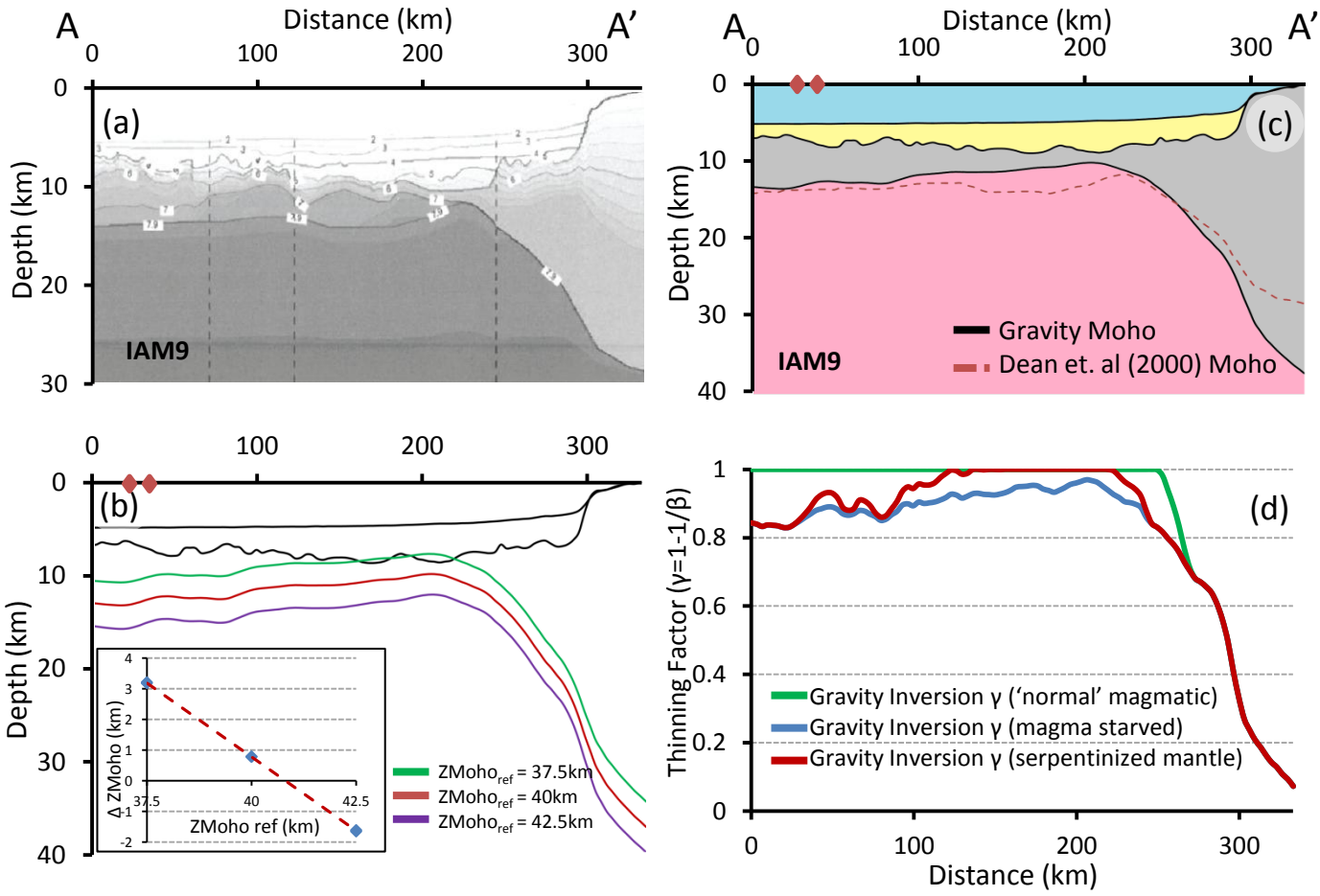

Figure 2 – Gravity anomaly inversion results. (a) Cross-section from wide-angle seismic data for IAM9 (Dean et al. 2000) showing Moho depth. (b) Moho depths predicted from gravity anomaly inversion using reference Moho depths of 37.5km, 40km and 42.5km. Inset shows the calibration of reference Moho depth. Difference (Δ ZMoho) between gravity anomaly inversion predicted Moho and seismic Moho depth (Dean et al. 2000) plotted against reference Moho depth. Calibration of the reference Moho depth gives a reference Moho depth of 41km. (c) Crustal cross section (A-A') along profile IAM9 constructed using bathymetry (Amante and Eakins 2009), 2D sediment thickness (Dean et al. 2000) and Moho depth from gravity anomaly inversion. The red dashed line shows the 7.9kms^{-1} iso-velocity contour (Dean et al. 2000) representing the seismic Moho depth. The red diamonds indicate the location of the Moho depths, in the oceanic domain, used for calibration. (d) Continental lithosphere thinning factors (γ) predicted from gravity anomaly inversion with sensitivities to a 'normal' magmatic solution, a magma-starved solution and a solution for serpentinised mantle.

Figure 3

Cowie, Kusznir & Manatschal 2015

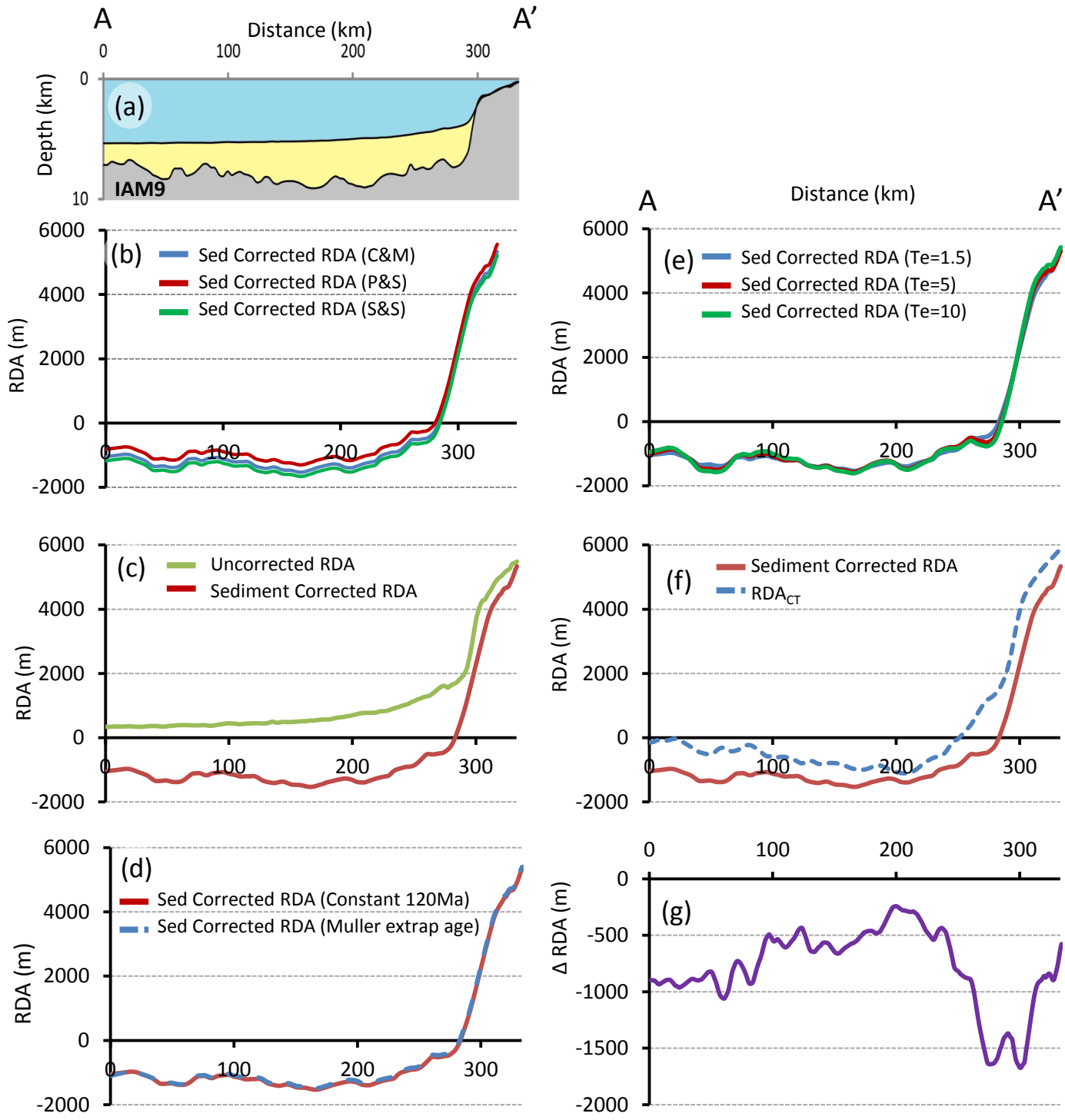

Figure 3 - (a) Bathymetry and depth to top basement for IAM9 profile. (b) Comparison of the residual depth anomaly (RDA) results computed using bathymetry-age predictions from Crosby and McKenzie (C&M) (2009), Parsons and Sclater (P&S) (1977) and Stein and Stein (S&S) (1992). (c) Comparison of uncorrected RDA results with the sediment corrected RDA results along IAM9. (d) The sensitivity to oceanic lithospheric age for sediment corrected RDA results examined using two approaches: the first uses a constant value of 120Ma for the profile, whilst the second uses Müller et al. (2008) age isochrons with their age gradient extrapolated inboard. (e) Sensitivities to the effective elastic thickness (Te) for the sediment corrected RDA results. (f) Comparison of sediment corrected RDA and the RDA component from crustal thickness variations (RDA_{CT}) along IAM9. (g) RDA corrected for sediment loading and crustal thickness variation.

Figure 4

Cowie, Kusznir & Manatschal 2015

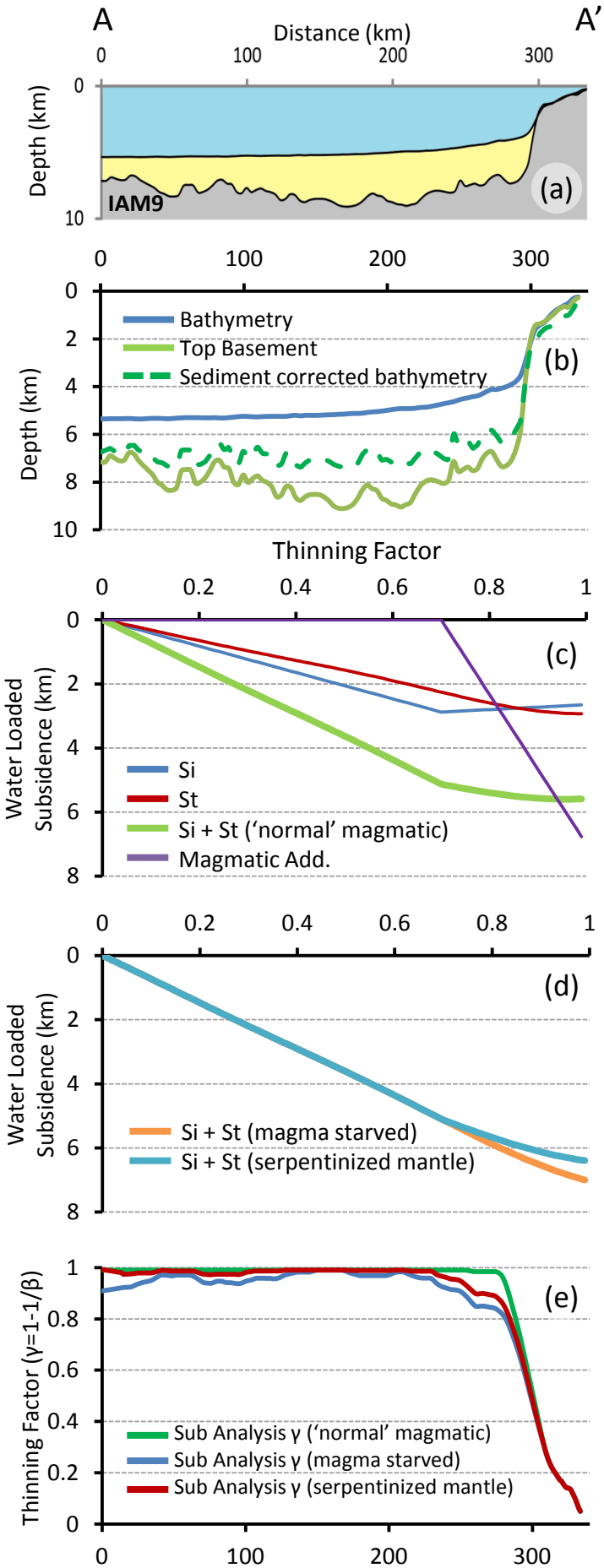

Figure 4 – Subsidence analysis involves the conversion of water loaded subsidence into continental lithosphere thinning factors, assuming McKenzie (1978), and is modified to incorporate the isostatic consequence of magmatic addition. (a) Bathymetry and depth to top basement for IAM9 profile. (b) Sediment corrected bathymetry determined by flexural backstripping of section (a). (c) Water loaded subsidence as a function of lithosphere thinning factor (γ) for a 'normal' magmatic solution. Initial subsidence (Si) is shown in blue, the time dependent thermal subsidence (St) is shown in red, the combined total subsidence (Si+St) is shown in green and the magmatic addition assuming decompression melting producing oceanic crust of 7km is shown in purple. (d) Water loaded subsidence as a function of lithosphere thinning factor (γ) for a magma-starved and a serpentinized mantle solution. (e) Continental lithosphere thinning factors (γ) from subsidence analysis along IAM9. Sensitivities to a 'normal' magmatic solution, a magma-starved solution and a solution for serpentinized mantle are shown.

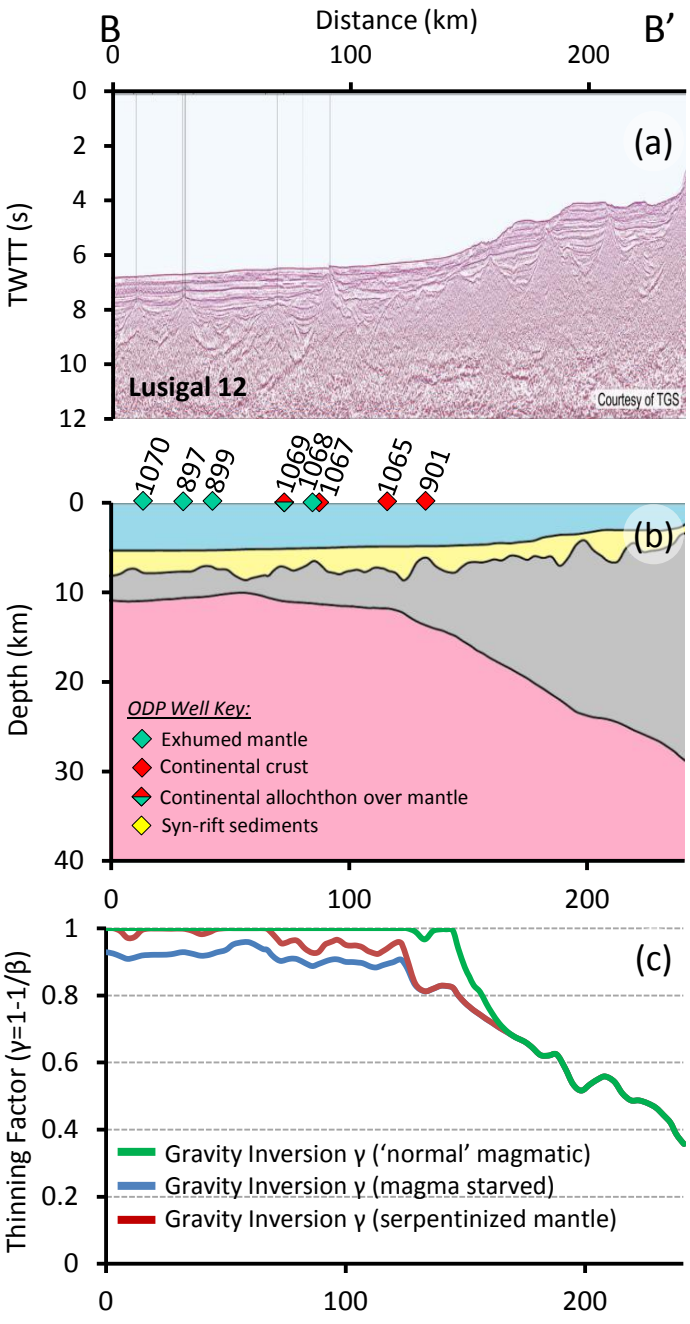

Figure 5 - (a) 2D seismic reflection profile (Sutra and Manatschal 2012) for Lusigal 12 (with the TGS extension). (b) Crustal cross section B-B' across Iberian Abyssal Plain, from gravity anomaly inversion. ODP well locations are identified and colour coded by crustal basement type. (c) Continental lithosphere thinning factors (γ) predicted from gravity anomaly inversion along Lusigal 12. Sensitivities to a 'normal' magmatic solution, a magma-starved solution and a solution for serpentinized mantle are shown.

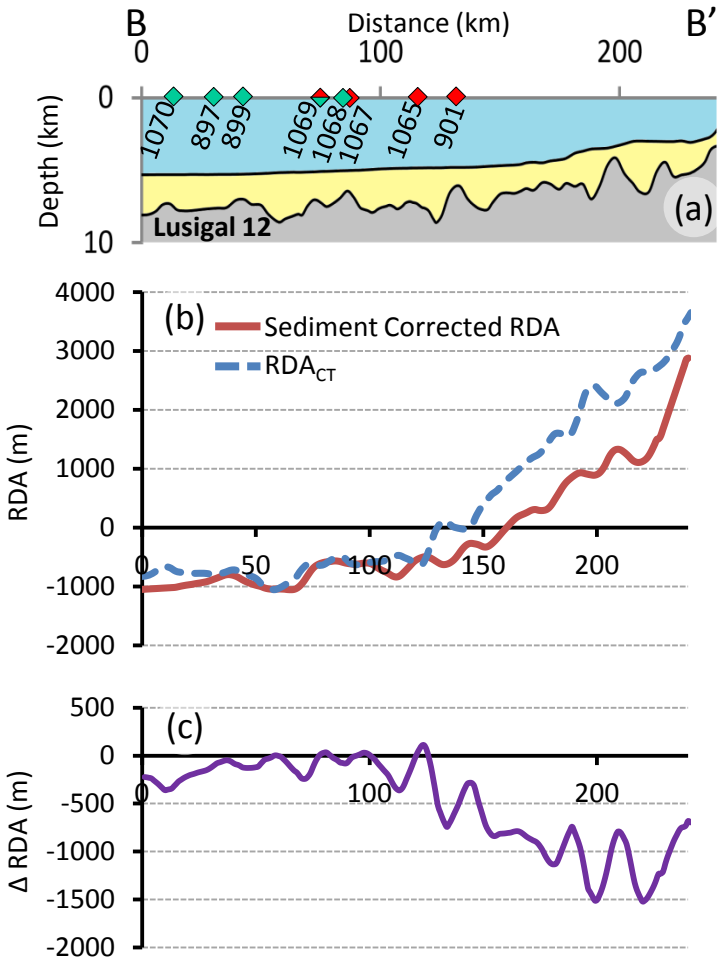

Figure 6 - (a) Bathymetry and depth to top basement for Lusigal 12. ODP well locations are identified and colour coded by crustal basement type (See ODP well key on Figure 5(b)). (b) Sediment corrected RDA and the RDA component from crustal thickness variations (RDA_{CT}) along Lusigal 12. (c) RDA corrected for sediment loading and crustal thickness variations.

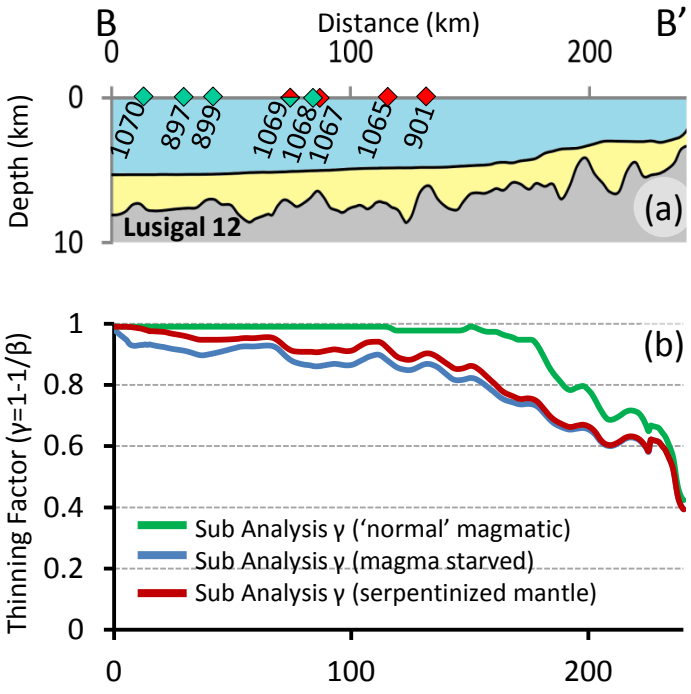

Figure 7 - (a) Bathymetry and depth to top basement for Lusigal 12. ODP well locations are identified and colour coded by crustal type (See ODP well key on Figure 5(b)). (b) Continental lithosphere thinning factors (γ) from subsidence analysis along Lusigal 12. Sensitivities to a 'normal' magmatic solution, a magma-starved solution and a solution for serpentinised mantle are shown.

Figure 8
Cowie, Kusznir & Manatschal 2015

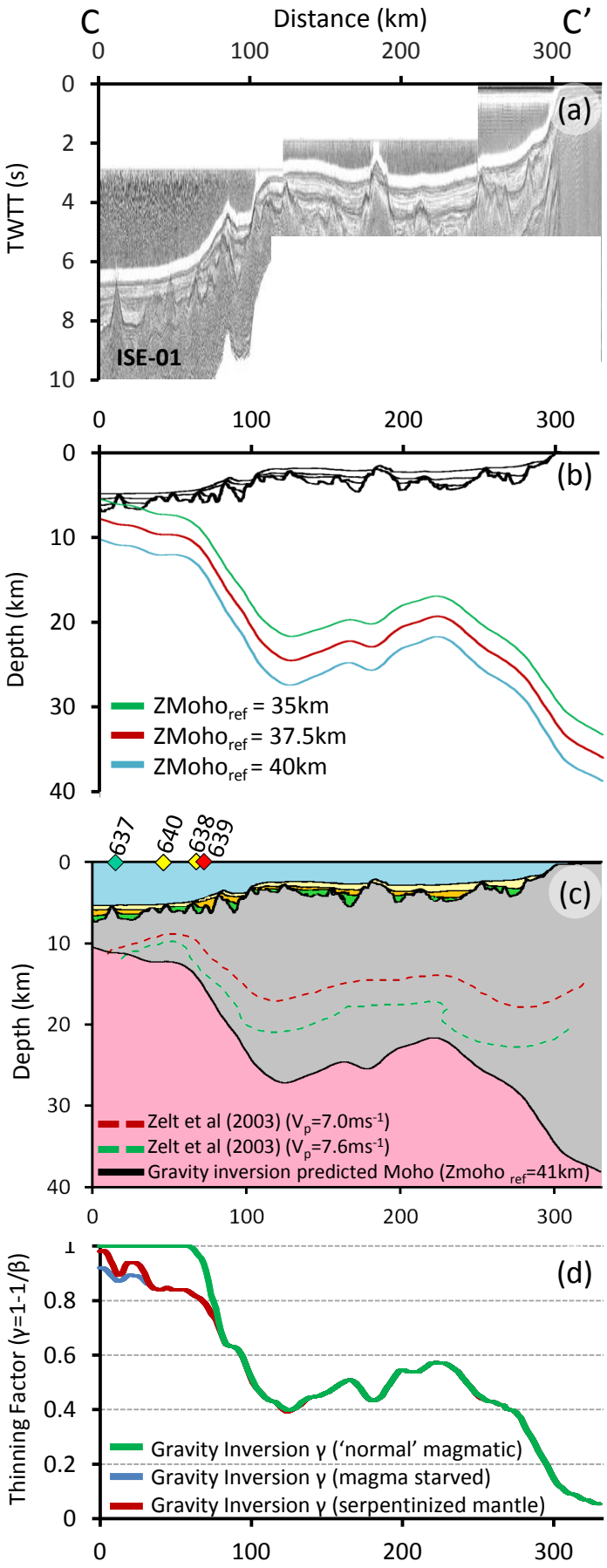

Figure 8 - (a) 2D seismic reflection data (from UTIG) along profile ISE-01. (b) Crustal cross section (C-C') along ISE-01 showing Moho depths predicted from gravity anomaly inversion, using reference Moho depths of 35km, 37.5km and 40km. (c) Crustal cross section (C-C') along profile ISE-01 using the calibrated reference Moho depth of 41km. The red dashed line shows the 7.0kms^{-1} iso-velocity contour and green dashed line shows the 7.6kms^{-1} iso-velocity contour (Zelt et al. (2003). ODP well locations are identified and colour coded by crustal basement type (See ODP well key on Figure 5(b)). (d) Continental lithosphere thinning (γ) from gravity anomaly inversion along profile ISE-01. Sensitivities to a 'normal' magmatic solution, a magma-starved solution and a serpentinised mantle solution are shown.

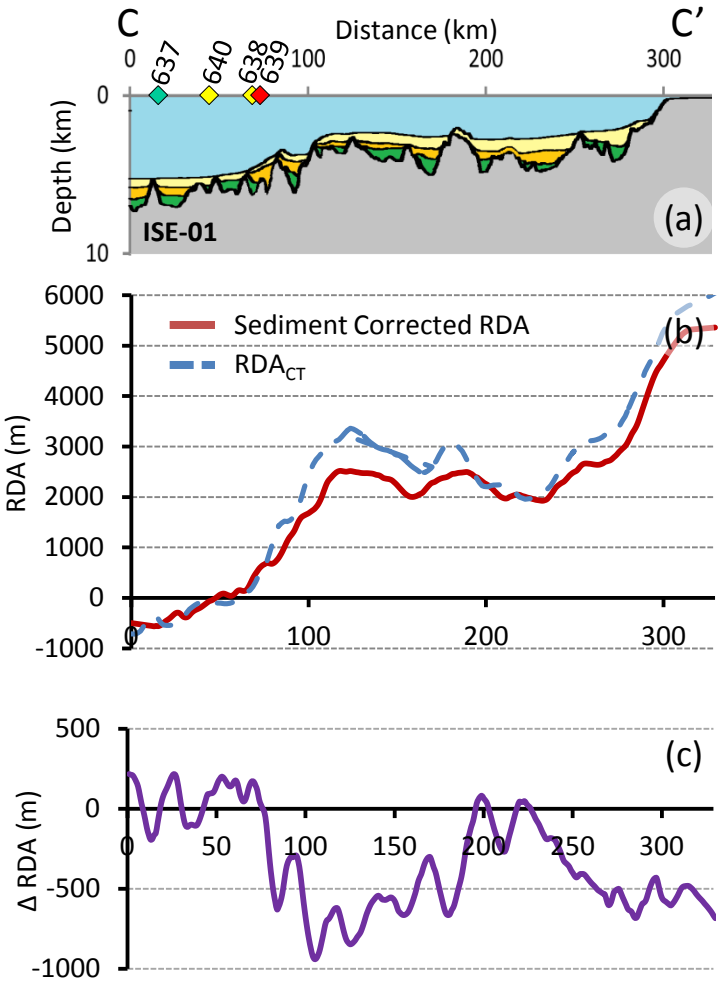

Figure 9 - (a) Bathymetry and depth to top basement for the ISE-01 profile. ODP well locations are identified and colour coded by crustal basement type (See ODP well key on Figure 5(b)). (b) Sediment corrected RDA and the RDA component from crustal thickness variations (RDA_{CT}) along ISE-01. (c) RDA corrected for sediment loading and crustal thickness variations.

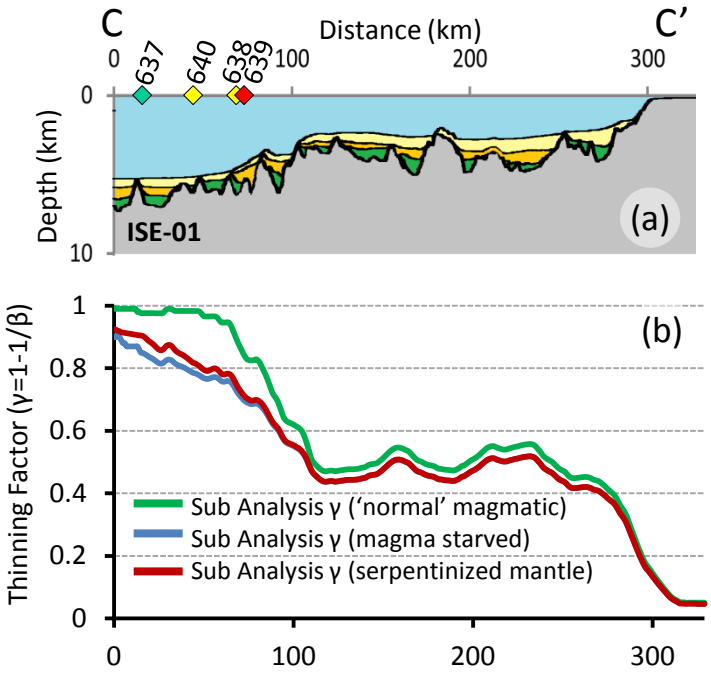

Figure 10 - (a) Bathymetry and depth to top basement for the ISE-01 profile. ODP well locations are identified and colour coded by crustal basement type (See ODP well key on Figure 5(b)). (b) Continental lithosphere thinning factors (γ) from subsidence analysis along ISE-01. Sensitivities to a 'normal' magmatic solution, a magma-starved solution and a solution for serpentinised mantle are shown.

Figure 11
Cowie, Kusznir & Manatschal 2015

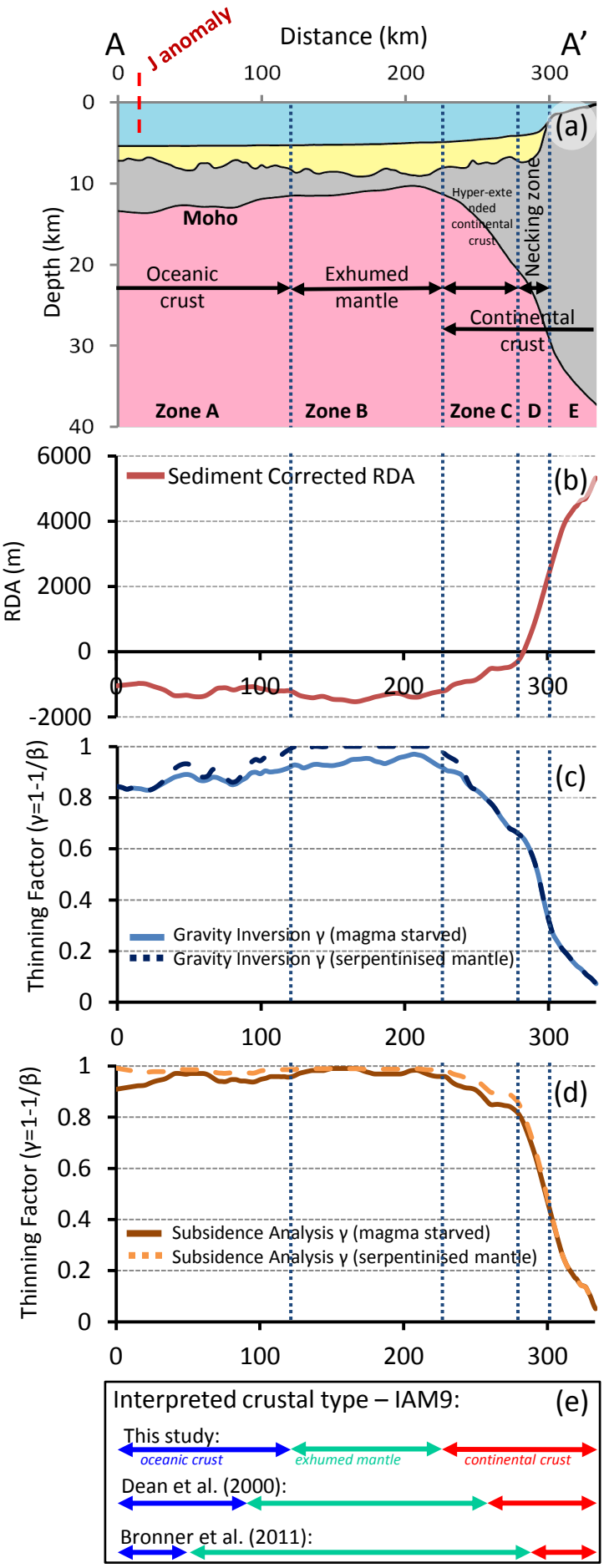

Figure 11 – Composite analysis plot along IAM9, showing interpretations of crustal basement types made from the integrated quantitative analysis. (a) Crustal cross section along profile IAM9 (A-A') from gravity anomaly inversion. The location of the J anomaly is indicated in red. (b) Sediment corrected RDA along IAM9. (c) Continental lithosphere thinning factors (γ) from gravity anomaly inversion assuming a magma-starved and a serpentinized mantle solution. (d) Continental lithosphere thinning factors (γ) from subsidence analysis assuming a magma-starved and a serpentinized mantle solution. Our interpreted boundaries between the crustal zones are indicated by the dashed lines. (e) Comparison of our interpreted crustal types with those from Dean et al. (2000) and Bronner et al. (2011).

Figure 12
Cowie, Kusznir & Manatschal 2015

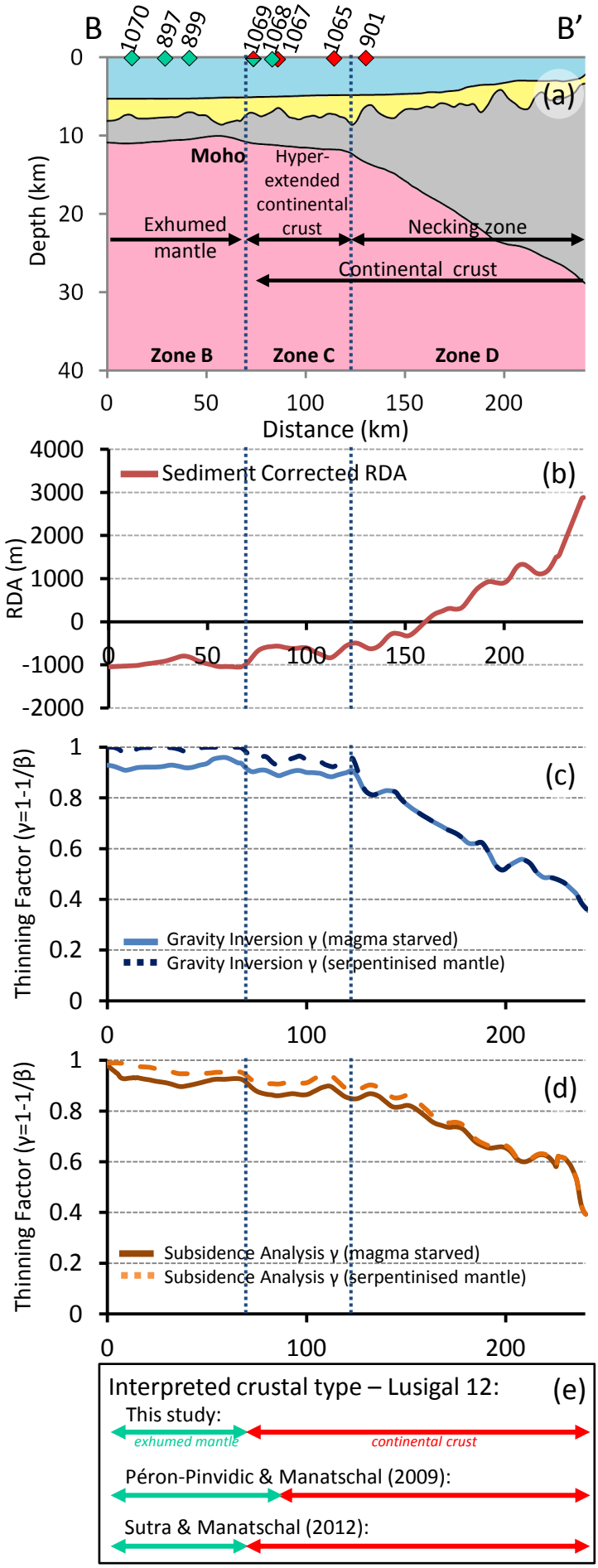

Figure 12 – Composite analysis plot along Lusigal 12, showing interpretations of crustal basement types made from the integrated quantitative analysis. (a) Crustal cross section along Lusigal 12 (B-B') from gravity anomaly inversion. ODP well locations are identified and colour coded by crustal type (See ODP well key on Figure 5(b)). (b) Sediment corrected RDA along Lusigal 12. (c) Continental lithosphere thinning factors (γ) from gravity anomaly inversion assuming a magma-starved and a serpentinized mantle solution. (d) Continental lithosphere thinning factors (γ) from subsidence analysis assuming a magma-starved and a serpentinized mantle solution. Our interpreted boundaries between the crustal zones are indicated by the dashed lines. (e) Comparison of our interpreted crustal types with those from Péron-Pinvidic & Manatschal (2009) and Sutra & Manatschal (2012).

Figure 13
Cowie, Kusznir & Manatschal 2015

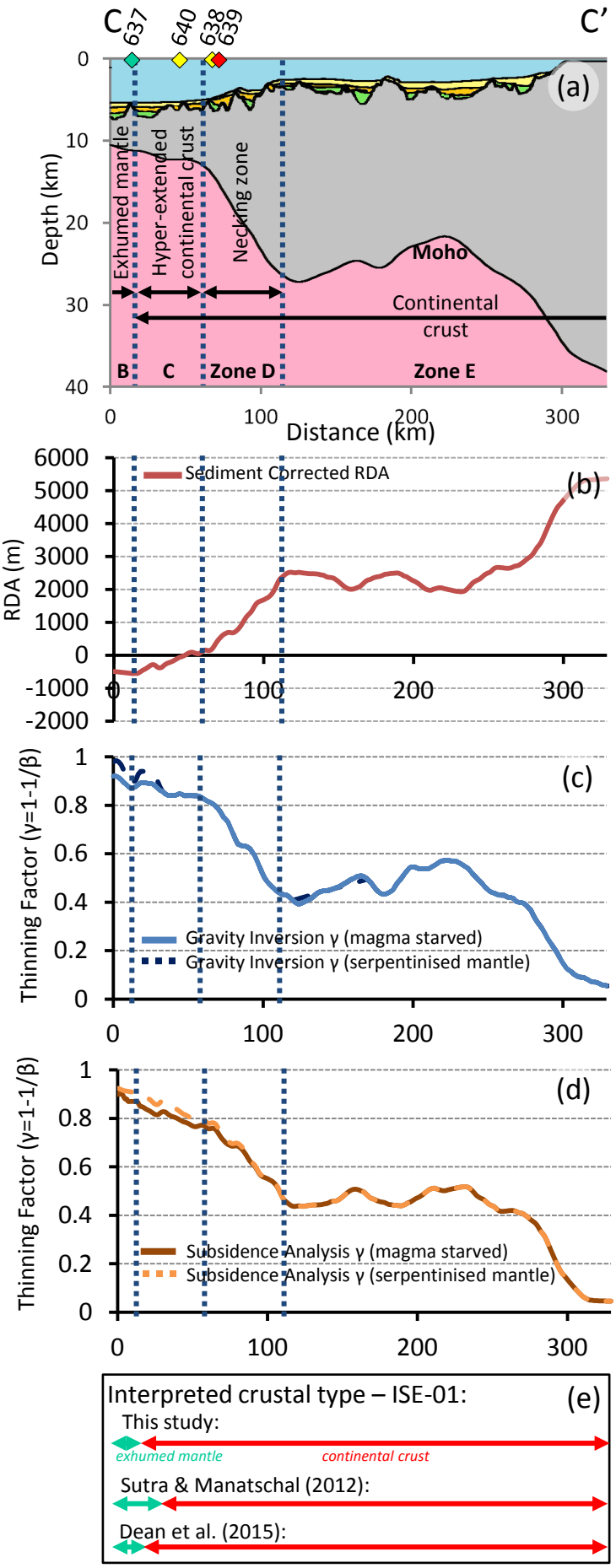

Figure 13 – Composite analysis plot along the ISE-01 profile, showing interpretations of crustal basement types made from the integrated quantitative analysis. (a) Crustal cross section along the ISE-01 profile (C-C') from gravity anomaly inversion. ODP well locations are identified and colour coded by crustal type (See ODP well key on Figure 5(b)). (b) Sediment corrected RDA along the ISE-01 profile. (c) Continental lithosphere thinning factors (γ) from gravity anomaly inversion assuming a magma-starved and a serpentinized mantle solution. (d) Continental lithosphere thinning factors (γ) from subsidence analysis assuming a magma-starved and a serpentinized mantle solution. Our interpreted boundaries between the crustal zones are indicated by the dashed lines. (e) Comparison of our interpreted crustal types with those from Sutra & Manatschal (2012) and Dean et al. (2015).